Development of an electric energy measurement node for agri-food industry sustainability assessment

Romina Eliana Giugge - 49194

Dissertation submitted to the School of Technology and Management of Bragança to obtain the Master Degree in Industrial Engineering

Scientific supervision:

Prof. Dr. João Paulo Coelho

Prof. Dr. Guillermo Gaston Riva

Bragança

2021-2022

Development of an electric energy measurement node for agri-food industry sustainability assessment

Romina Eliana Giugge - 49194

Dissertation submitted to the School of Technology and Management of Bragança to obtain the Master Degree in Industrial Engineering

Scientific supervision:
Prof. Dr. João Paulo Coelho
Prof. Dr. Guillermo Gaston Riva

Bragança
2021-2022

Dedication

I dedicate this work to my mother Marcela, my father Daniel and my brother Marcos. The support I received from my family made this possible and I am eternally grateful to them for encouraging me to fulfill my dreams and for always being present despite the distance. Without them, none of this would have been possible.

Acknowledgment

I would like to thank all those people who in any way contributed to the development of this work.

First, to my supervisor at the Instituto Politécnico de Bragança (IPB), Professor Dr. João Paulo Coelho, for all the support throughout this work, for guiding me and teaching me at every step. I am very grateful for the experience gained throughout this year. Thank you so much.

I also want to thank my supervisor at the Universidad Tecnológica Nacional, Facultad Regional Córdoba (UTN-FRC), Professor Dr. Guillermo Riva, for his support and for always being willing to answer my questions in each email.

To my home university, UTN-FRC, for the opportunity to participate in the Dual Diplomacy program and for all the learning throughout my course.

Last, but not least, I want to thank my family and friends. Specially to my parents and brother for always supporting me, for accompanying me and for being present even from a distance. None of this would have been possible without them. Eternally grateful.

Abstract

The characterization of the sustainability of both products and processes is an emerging social and political concern due to the increase in population and the stress that this fact imposes on the available natural resources. In order to counteract this problem, the European project BIOma- Integrated BIOeconomy Solutions for the Mobilization of the Agri-food Chain aims, in one of its objectives, to establish a sustainability indicator designated by siBIO. This sustainability index can be requested by any agri-food company and, in order to be granted, an audity process takes place where a set of operational conditions are evaluated during a given time horizon. Among them, water and energy consumption, at several points in the processing chain, must be monitored. In this context, this work proposes the implementation of a Internet of Things (IoT) measurement device which integrates LoRa based communication abilities and capable of monitoring the consumption of electrical energy in real-time. Thereby, a microcontrolled based system was developed to carry out measurements using a custom-made current sensor whose data is sent to a FIWARE context management where the siBIO information infrastructure can access it remotely. Details regarding the design and calibration of the custom-made electric current sensor is provided and, according to the lab results obtained, the measurement node developed was able to operate as expected.

Keywords: Internet of Things; LoRa; Current Sensor; Sustainability; BIOMA project.

Resumo

A caracterização da sustentabilidade de produtos e processos é uma preocupação social e política emergente devido ao aumento da população e ao stress que esse fato impõe aos recursos naturais disponíveis. Para contrariar este problema, o projeto europeu BIOma-Integrated BIOeconomy Solutions for the Mobilization of Agri-food Chain visa, num dos seus objetivos, estabelecer um indicador de sustentabilidade designado por siBIO. Este índice de sustentabilidade pode ser solicitado por qualquer empresa agroalimentar e, para ser concedido, é realizado um processo de auditoria onde são avaliados um conjunto de condições de funcionamento durante um determinado horizonte temporal. Entre eles, o consumo de água e energia em vários pontos da cadeia de produção e transformação deve ser monitorado. Neste contexto, este trabalho propõe a implementação de um dispositivo de medição IoT que integra capacidades de comunicação baseadas em LoRa e capaz de monitorizar o consumo de energia elétrica em tempo real. Assim, foi desenvolvido um sistema baseado num microcontrolador para realizar medições utilizando um sensor de corrente feito sob medida cujos dados são enviados para um gerenciador de contexto FIWARE onde a infraestrutura de informações do siBIO pode aceder remotamente. Detalhes sobre o projeto e calibração do sensor de corrente elétrica são apresentados. De acordo com os resultados laboratoriais obtidos, o nó de medição desenvolvido foi capaz de operar conforme o esperado.

Palavras-chave: Internet das Coisas; LoRa; Sensor de Corrente; Sustentabilidade; BIOMA project.

Contents

List of Tables

List of Figures

Acronyms

AC Alternating Current.

AJAX Asynchronous JavaScript and XML.

API Application Programming Interface.

BMS Battery Management System.

CNC Computer Numerical Control.

DC Direct Current.

HTML Hypertext Markup Language.

IoT Internet of Things.

IP Internet Protocol.

IPv6 Internet Protocol version 6.

JSON JavaScript Object Notation.

MQTT Message Queuing Telemetry Transport.

OA Operational Amplifier.

PCB Printed Circuit Board.

PHP Hypertext Preprocessor.

RMS Root Mean Square.

SCADA Supervisory Control And Data Acquisition.

SCC Signal Conditioning Circuit.

SE Standard Error.

SOGI Second Order Generalized Integrator.

SPI Serial Peripheral Interface.

WAN Wide Area Network.

WSN Wireless Sensor Network.

Chapter 1

Introduction

This chapter aims to present the general motivation of the work, enumerate its objectives and define the document structure adopted.

1.1 Overview

All processes that use, in some way, the natural resources of our planet are continually under political and social pressure to be more efficient [1]. Currently, there is no certification process for agri-food holdings implemented in the market for the issue of sustainability, so the BiOMA project intends to work on a digital solution. This will allow to assess the level of sustainability of companies in the agri-food chain, namely primary production (agriculture), transformation (industry) and logistics.

Carried out under the project "BIOMA – Integrated Bioeconomy Solutions for the Mobilization of the Agri-food chain", by the "BIOMA" Consortium, financed by the European Regional Development Fund (ERDF), through the Incentive System for Technological Research and Development, within the scope of of the Portugal2020 Operational Program for Competitiveness and Internationalization.

It is a Portuguese project coordinated by Conservação e Transformação de Hortofrutícolas, S.A. (CAMPOTEC) and with the collaboration of the Instituto Politécnico de Bragança (IPB), BRIDGEPOINT, Instituto Politécnico de Santarém (IPS), Instituto Politécnico de Viana do Castelo (IPVC), Laboratório Colaborativo Montanhas de Investigação – Associação (MORE) and Sociedade Geral de Superintendência S.A. (SGS), whose objective is the complete characterization of the production processes, to collect measured quantities and various parameters necessary to take advantage of the automation of the siBIO sustainability index. In addition to carrying out an analysis of the necessary requirements to carry out the digitization and sensorization of primary production systems.

To obtain the seal of sustainability, it requires the computation of a set of figures of merit that depend on the information provided by a wide set of variables of different types. In the context of siBIO, the type and scope of these variables is defined at various hierarchical levels, one of them being where the variables that can be automatically collected through sensor networks with a certain cadence are identified.

Currently, using Wireless Sensor Network (WSN) has presented a notable increase due to the fact that these systems allow capture information on the geographic area in which they are deployed and because they are formed by autonomous devices, used for monitoring over a space of physical and environmental variables. They are also based on modules that are easily manipulated that allow networks to have improvements and modifications in their operation.

The integration of WSN with IoT allows applications to communicate with each other and users on a global scale since the latter enables control, communication and collaboration with several hardware devices over computer networks. The main advantages of the IoT are: ease of access to information, greater efficiency and productivity, energy savings, more sustainable processes, direct communication with the environment and, of course, the ability to connect to the internet.

1.2 Motivation

The work presented in this thesis arises from the BiOMA project, in which the IPB is a part since it acts in an integrated manner to meet the needs of the community by providing resources that contribute to local development from a perspective of continuous improvement and innovation.

The main objective of the BIOMA project is to reposition diverse companies on competitive and sustainable levels. The IPB, through areas of social action, culture and education, among others, develops its activity with the aim of providing the population with services and social responses from a perspective of continuous improvement and innovation.

This project arises from the need to be more aware of the environment, to be a more sustainable production process and improve as much as possible. Although it is intended to do something in general terms, the main objective is to make it possible to choose what is most relevant according to the place where the different sensor networks will be implemented.

As discussed in [2], it is necessary to say that all industries have the same problem due to the heterogeneity of the systems involved. Currently it is possible to find many studies on the design and analysis of a sensor network to be applied in various areas, but most of them base their design according to the environment where they will be applied and the needs. The objective of this work is to create a LoRa node whose function is to obtain data on the energy consumption of a component and which in turn can be applied in any industry.

1.3 Objectives

The challenge for this thesis is to create a prototype of a LoRa node capable of obtaining information and sending it to a server where a subsequent analysis and calculations will be carried out, necessary to determine the sustainability of the supply chain where they

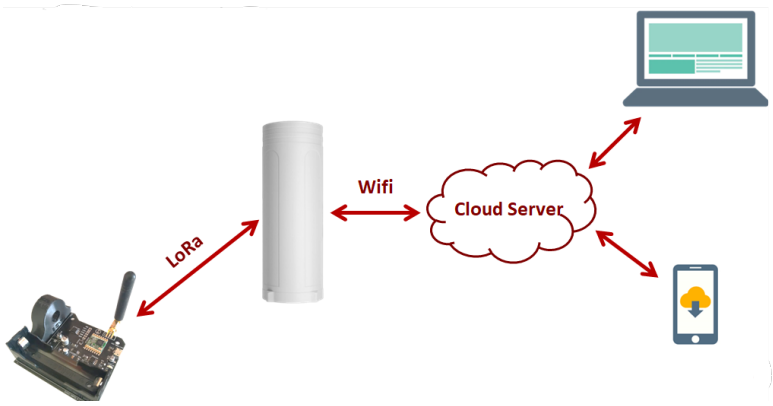

Figure 1.1: Architecture of the objective.

were applied.

The main objective is to work on the custom-made current sensor, its calibration and tuning, and to be able to implement a code in a microcontroller for this to send the collected data to a FIWARE context management. Particularly, the challenge is to measure the energy consumed and send those measurements to a FIWARE context management, where the siBIO information infrastructure can access it remotely.

Furthermore, the microcontroller and sensor must be integrated in such a way that it can be installed into the existing environment where it is required. Thereby, it is expected that the system provides a useful and reliable solution that monitors, calculate the calculate electrical energy and send these results for, as mentioned above, to be analyzed. So, the system is expected to provide a useful and reliable solution that monitors and records the consumption of electrical energy and send such data periodically.

1.4 Document Structure

This document is organized in 6 chapters, where the present chapter presents the motivation and objectives of the work.

Chapter 2 presents a bibliographic review, which addresses content necessary to understand the concepts used for the process of creating the work and the implemented system.

Chapter 3 begins with the presentation of the current sensor, where the calibration process and the different results obtained throughout the process are shown, as well as the microcontrollers that were part of the analysis.

Chapter 4 shows the implemented solution, with a description of the Hardware and Firmware developed for this purpose.

Then, Chapter 5 presents overall considerations regarding the solution adopted in addition to the price list of the LoRa node developed.

Finally, chapter 6 outlines the main conclusions and points out the future work.

Chapter 2

Related Work

This chapter presents the State of Art, that is, the bibliographic review necessary to understand the concepts of IoT and current measurement systems. Section 2.1 presents the definition, progress and challenges of IoT and finally the basic architecture of a typical IoT system with its tasks and functions. Followed by Section 2.2, which presents a few studies about the concerns regarding IoT and its implementation in web development. Section 2.3 highlight the wide range of methods used in the measurement of electrical current, and finally, Section 2.4 exposes some of the methods for the calculation of Root Mean Square (RMS) current and the use of algorithms of low computational cost.

2.1 Internet of Things

The Internet of Things is a concept that refers to the technology that allows everyday objects to be connected to the Internet, giving them the capacity so that they can exchange information with each other.

The uses of the IoT are very broad, among them stand out: domotics, automation and control of production processes; transport and logistics; agriculture, livestock and forestry; medicine and health care; video surveillance and security, among many others. The advantages and disadvantages of the internet of things are varied and important that must be taken into account when choosing it. The advantages offer us great possibilities and

benefits, such as we already mentioned above, energy and economic savings, the possibility of connecting to the Internet, greater sustainability and the possibility of exchanging information quickly and in real time, among many others. However, the disadvantages present us with an iffy scenario where we are not in control in the way that we would like. For example, the IoT cannot ensure that our data does not reach the wrong hands, the information is not encrypted, there is no compatibility between some devices and not to mention the technological gap that exists in the world. However, despite the disadvantages of this technology, the IoT is here to stay and, consequently, we will have to improve it and know how to adapt it to make the most of it while minimizing its possible risks.

The massive evolution of the IoT occurred mainly due to the improvement of some technologies, e.g., wireless network, wide adoption of Internet Protocol (IP), cloud computing alongside with cost reduction in storage systems, lowered cost of computing and communications devices [3]. The solutions used for IoT Systems create a complexity environment due the numerous use of several technologies which is rapidly changing [4]. Many articles propose standard solutions for IoT as addressed by [5]–[9], however, these are based on pre-established sensors and nodes, so there are still those who wonder if it is possible to create their own sensor according to a particular need, common standards that improve questions about connectivity, interoperability, security and privacy, return on investment, and social questions regarding IoT system development.

Beyond all the challenges of the IoT, there are a lot of domains which have a positive economic impact with the growing use of the technology, e.g., healthcare, manufacturing, electricity, smart city, security, etc [9].

2.1.1 IoT Architecture

As the IoT systems are gaining popularity, it becomes important to know and understand its structure, which can be described as a four-stage process in which data flows from the sensors connected to the "Things" through a network to a corporate data center for processing, analysis and storage (Figure 2.1).

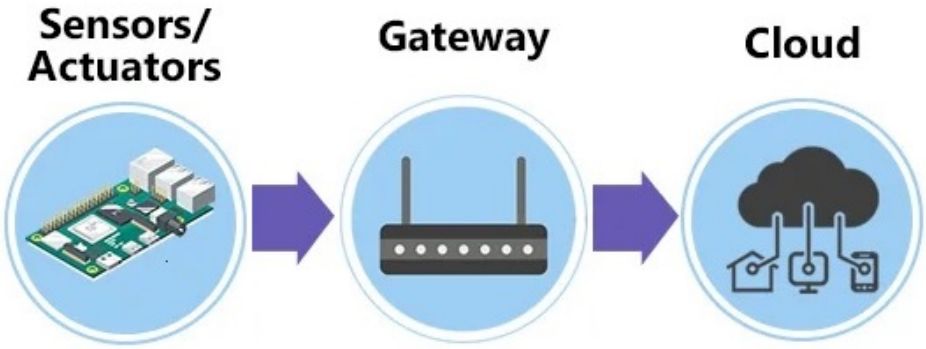

Figure 2.1: IoT Architecture.

The process begins with sensors (those connected devices that monitor) and actuators (those that control) some "Thing" or physical process. A data acquisition system collects the raw data from the sensors and converts it from analog to digital format. The system formats the data before sending it over an Internet gateway over a wireless Wide Area Network (WAN) (such as Wi-Fi or cellular) or a wired WAN for the next stage of processing. At this point, the data volume is at its maximum, so the data is filtered and compressed to an optimal size for transmission. Once the data has been digitized it needs to be processed to further reduce the volume before it goes to the data center or the cloud. In the final phase of the process, computer systems can be used to analyze, manage and store the data securely. At this level, industry and/or company-specific applications can also be used to perform in-depth analysis and apply business rules to determine whether or not action is necessary. Incoming data can indicate desirable changes to device settings or other ways to optimize the process, forming a loop that facilitates constant improvement.

2.2 Web Development applied to IoT

Due to the massive growth of the Internet, Internet-based applications are becoming more and more popular in both the business world and industry. [10] presents the design of an intelligent remote electrical power Supervisory Control And Data Acquisition (SCADA) system based on IoT.

Web technology is widely used in managing the data collected by IoT devices as any network of connected devices relies on web servers and cloud storage to operate. In turn, a user interface is needed so that any client can access such data and can interact with the connected devices. The use of Asynchronous JavaScript and XML (AJAX) technology in combination with Hypertext Markup Language (HTML), JavaScript and Hypertext Preprocessor (PHP) was recently proposed in the context of IoT [11]. The work is based on the client-server paradigm, where the server applications manage the data collected by the IoT devices, storing them in a database and thus allowing the client to access them in real time.

Since IoT technology is an interconnected network it is susceptible to hacking, therefore developers must adopt practices to ensure security [12]. Recently, [13] presents the challenges of implementing a secure IoT application from a maker perspective. Issues with security of the Message Queuing Telemetry Transport (MQTT) session were also investigated and discussed.

Another important factor in the integration of web development in IoT is related to the scalability and security of the system. [14] illustrates the scalability of a system designed with a dynamic scaling mechanism and compares it to those based on a static, fixed pool of service instances. In turn, [15] presents an analytical perspective on the scalability of Internet Protocol version 6 (IPv6) to address the huge growth of IoT. There it is shown that the addressing capacity of IPv6 is sufficient to satisfy communication needs.

A recent survey by the Eclipse Foundation [16] revealed that security (46 %), connectivity (38 %) and deployment (31 %) are the top concerns for IoT developers in 2021. In addition, the survey found that communication security (43 %), data encryption (27 %) and anomaly detection/analysis (22 %) are the technologies related to the most widely used security and that MQTT has emerged as the leading protocol for IoT communication (44 %), showing solid growth over the last year.

2.3 Methods Used in Current Measurement Systems

Electric current consumption is an important parameter to take into account. Knowing the consumption of either an appliance in the home or machinery in the industry allows us to know if the energy consumption is very high and if it is necessary to resort to an energy saving plan and even allows us to detect problems making it possible also find solutions.

In 1999, [17] presents various solutions suitable for measuring high currents that are typical in power electronic devices such as motor inverters, welding power supplies, induction heating devices, etc. The accuracy and suitable applications of each current measurement system are discussed. The methods addressed are: shunt resistors, current transformers, Hall sensor alongside other magnetic field sensor. It also presents accuracy and appropriate applications of each system.

In 2009, [18] exemplifies and compares some methods for measuring electrical current consumption in a smart grid. Among the different methods to measure the magnetic field are force, magnetoresistance, gian magnetoimpedance, Hall effect, Direct Current (DC) current transformer, the current comparator, magnetostriction and Faraday effect. However, the number of current sensors that will be needed will far exceed the number now in the transmission system. Current measurement will become big business [18].

Current measurement is used for control, protection, monitoring, and power management purposes. Parameters such as low cost, accuracy, high current measurement, isolation needs, broad frequency bandwidth, linearity and stability with temperature variations, high immunity to dv/dt, low realization effort, fast response time, and compatibility with integration process are required to ensure high performance of current sensors. In [19], various current sensing techniques based on different physical effects such as Faraday's induction law, Ohm's law, Lorentz force law, magneto-resistance effect, and magnetic saturation are studied.

It can be seen that there are several methods for measuring electrical current, each with its advantages and disadvantages, being more beneficial for certain applications and

not so much for others. However, currently it is not so easy to find an application where the current sensor to be used can be adapted to any type of application or that in turn is incorporated into a network of LoRa sensors.

2.4 Method For Calculating RMS Current

By definition, the effective value is the root mean square of the instantaneous values over a full period. Equation 2.1 shows the RMS current calculation (I_{RMS}), where $i(t)$ is the value of the instantaneous current and T represents the period of the signal.

$$I_{RMS} = \sqrt{\frac{1}{T}\int_0^T i^2(t)dt} \tag{2.1}$$

Conventional algorithms use sequential samples with sampling frequency equal to N times the Alternating Current (AC) frequency, therefore, they consider N to be constant and integer, but when the actual frequency is not exactly the nominal one, errors are introduced in the calculations. The purpose of [20] is to present a method to minimize these errors by making N a variable and not an integer.

On the other hand, [21] compares the performance of the cosine filter method and the Second Order Generalized Integrator (SOGI) method in calculating RMS voltage and current for system fault detection.

For the first calculations of I_{RMS} in this work, the method chosen was the numerical approximation of the integral of Equation 2.1, using the rectangular approximation, which leads us to redefine it as shown in Equation 2.2, where N is the number of partitions taken in the period T and T_s is the sampling period.

$$I_{RMS} = \sqrt{\frac{1}{N}\sum_{k=0}^{N-1} i(kT_s)^2} \tag{2.2}$$

Begin Equation 2.2 the one that is going to be implemented in the software used for the tests made with the HST023R sensor for the calculation of I_{RMS}. Such software can be found in Appendix B.

Currently there are proposals that use hardware with limited resources or the classic formulas of RMS to analyze the current consumption. So, [22] presents an approximation using a RMS value estimator that uses a low-cost basic range microcontroller as a base, with low computational cost calculation algorithms.

Chapter 3

Materials and Methods

This chapter presents the technological tools used for the development of this work and the different stages of testing until reaching the final node. Section 3.1 gives a brief introduction to the current sensor used initially, its calibration process, the calculations and results of the first SCC implemented. Followed by Section 3.2 with a similar analysis but for a second version of the SCC. Then, Section 3.3 shows the design of a digital inverse notch filter necessary for data collection. Section 3.4 shows the measurement results and, finally, Section 3.5 presents the process of designing, creating and calibrating of the custom current sensor.

3.1 Hall Split Core Current Sensor HST023R

Figure 3.1: Hall Split Core Current Sensor.

As mentioned formerly, the objective of this work is to sense the current consumed in order to obtain information on how much the consumption is per day. For this, it was first chosen to work with the HST023R current sensor since it is of the Open loop split core type, which means that it can be easily installed in any industry, factory or premises that want to monitor without the need to cut cables or carry out a special installation.

Some of the main characteristics of the sensor are: light weight, low power consumption, fast response time, good anti-interference ability and good linearity.

As can be seen in the datasheet included in the Appendix A, the sensor has four cables, three of which are for the power supply and one of them is the sensor output which provides an output voltage (V_{out}) proportional to the measured current.

According to the technical specifications of this sensor, it is capable of offering an output between -4V and 4V, so it was necessary to carry out a series of measurements to be able to calibrate and know the behavior of the sensor. Said procedures and results will be shown in Section 3.1.3.

3.1.1 Method Used for the Current Sensor Calibration Process

The calibration process of this sensor involved performing a sequence of tests where different values of electrical current were injected into an electrical conductor that passed through the clamp and the voltage values at the sensor output were recorded.

Due to the fact that the measurement range covered by the sensor is very wide and that the sensor will be applied to measure AC type current, it was necessary to resort to different elements that could provide different current values. In the first instance, two heaters, a hair dryer and three low-power lamps were used, which were turned on in groups to reach different current values. To be able to reach intermediate values, it was necessary for the driver to pass through the sensor several times, as, for example, shown in Figure 3.3(a).

In order to be able to carry out the measurements in a quickly and easy way, a device consisting of lamps of different powers was created, these being 120W, 240W, 600W and

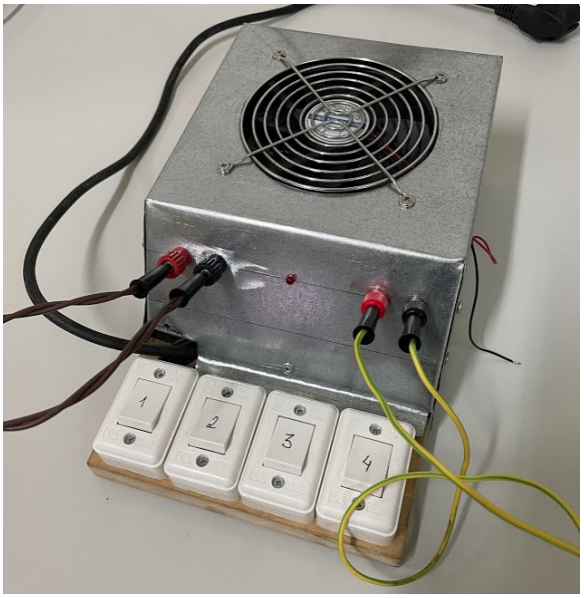

Figure 3.2: Device Used for the Calibration Process.

1000W. It also implies $2^4 - 1 = 15$ possible combinations, which can be seen in Table 3.1. Such a device is shown in Figure 3.2, where it can be seen a red LED in the middle with the aim of alerting if the phase is connected to the cable on the left, that is, for safety. Said cable can be replaced by a multimeter or it can be measured with an amperometric clamp in order to reliably know how much current is being delivered by the device.

The cable on the right is the one that will be surrounded by the current sensor in order to obtain the voltage values at its output. Lastly, it can also be seen four switches used to create different on/off combinations to achieve different current values.

This device is capable of delivering a maximum current of approximately $7 - 8A$, allowing different combinations to achieve wide ranges of values. The only disadvantage is that this type of lamp overheats a lot, so it does not allow long measurements in time. That is, it becomes necessary to take pauses and take measurements quickly, but it was still a great solution for the calibration process.

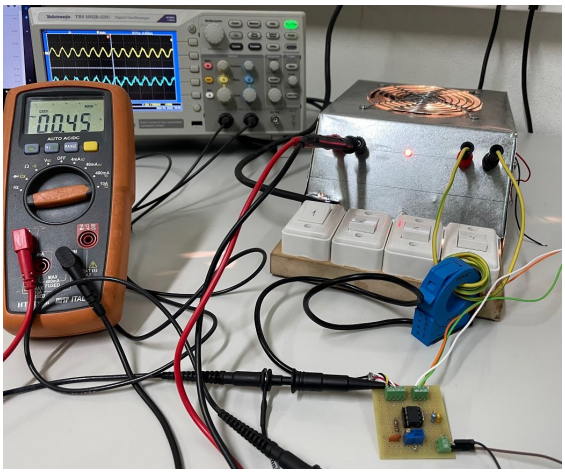

(a) Method for Measuring Intermediate Current Values.

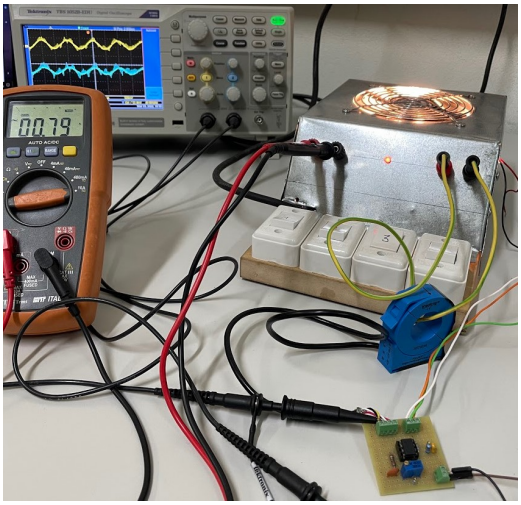

(b) Method for Measuring Current Values.

Figure 3.3: Calibration Method.

Switch Number	**Current Value [A]**
1	0.45
2	0.85
1 - 2	1.3
3	2.67
1 - 3	3.12
2 - 3	3.52
1 - 2 - 3	3.97
4	4
1 - 4	4.45
2 - 4	4.85
1 - 2- 4	5.3
3 - 4	6.67
1 - 3 - 4	7.12
2 - 3 - 4	7.52
1 - 2 - 3 - 4	7.97

Table 3.1: Approximate Current Values due to Different Ignition Combinations.

3.1.2 Signal Conditioning Circuit V.1

Thanks to the sensor datasheet it was possible to know in advance that the possible values of V_{out} were between -4V and 4V, however the Arduino board inputs only admit values between 0V and 5V so it was necessary to design a conditioning circuit signal for that

matter. For this, the Operational Amplifier (OA) was used in its Differential configuration to adjust the output values according to those necessary. The circuit is the one shown in Figure 3.4. Since the current sensor is powered with ±15V, the TL082 was chosen since it can also be powered with these values and the negative voltage will be used as a reference.

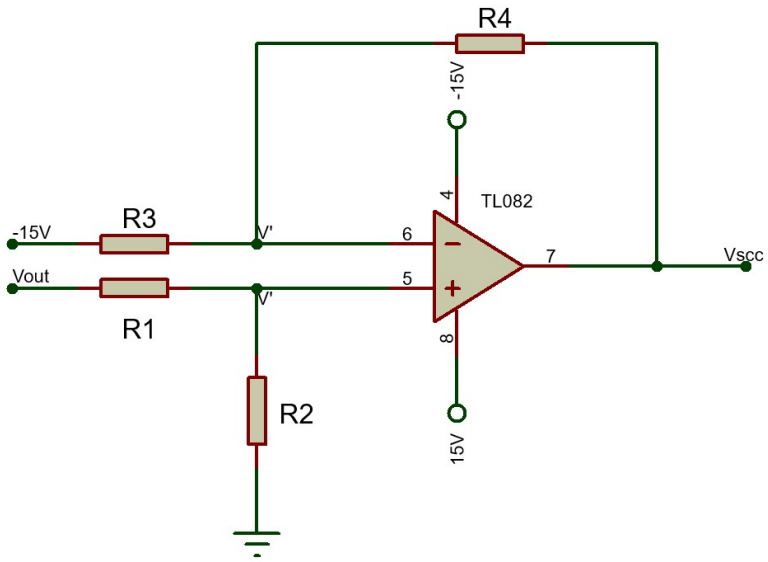

Figure 3.4: Differential Amplifier.

Due to the properties of the OA, we can establish a V' that will be the same in both inputs and that by observing the configuration of the circuit in the non-inverting input we can obtain its value as follows:

$$V' = \frac{R_2}{R_1 + R_2} V_{out} \tag{3.1}$$

Where V_{out} is the signal at the sensor output.

At the same time, the current at the non-inverting input is the same as the current in the feedback loop due to the high impedance that the OAs present at their input, so the following expression is obtained:

$$\frac{V_{ref} - V'}{R_3} = \frac{V' - V_{scc}}{R_4} \tag{3.2}$$

Rearranging terms and solving:

$$\frac{-V_{scc}}{R_4} + \frac{V'}{R_4} = \frac{V_{ref}}{R_3} - \frac{V'}{R_3} \tag{3.3}$$

$$\frac{-V_{scc}}{R_4} = \frac{V_{ref}}{R_3} - \frac{V'}{R_3} - \frac{V'}{R_4} \tag{3.4}$$

$$-V_{scc} = V'(\frac{1}{R_3} + \frac{1}{R_4})R_4 - \frac{V_{ref}}{R_3}R_4 \tag{3.5}$$

With $V_{ref} = -15$ and replacing V' by the expression obtained in Equation 3.1, we would have:

$$V_{scc} = V_{out}(\frac{R_2}{R_2 + R_1})(\frac{R_4 + R_3}{R_3}) + 15\frac{R_4}{R_3} \tag{3.6}$$

In order to solve Equation 3.6, it is necessary to establish a relation between the possible output values of the current sensor and the possible input values of the Arduino board, for this the graph shown in Figure 3.5 was made and whose equation is the following:

$$V_{scc} = \frac{5}{8}V_{out} + \frac{20}{8} \tag{3.7}$$

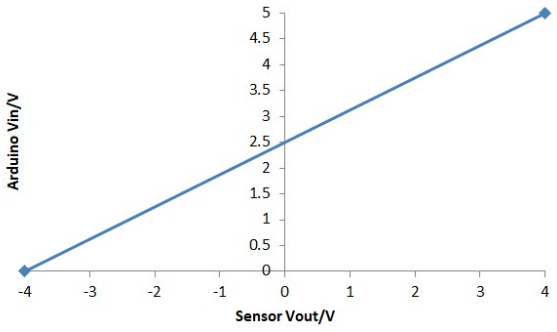

Figure 3.5: Relation between Vout and the possible input values of the Arduino board.

Equating the Equation 3.6 with 3.7 we can obtain the following correlations:

$$15\frac{R_4}{R_3} = \frac{20}{8} \tag{A}$$

$$(\frac{R_2}{R_1+R_2})(\frac{R_4+R_3}{R_3}) = \frac{5}{8} \tag{B}$$

$$1K\Omega < R < 100K\Omega \tag{C}$$

Furthermore, in any application of OAs it is preferable to keep the resistance values in the range defined by C, in this way we establish the values of $R_2 = 10K\Omega$ and $R_3 = 10K\Omega$. To obtain the values of R4, Equation A is solved as it's shown in Equation A.1. To obtain the value of R1, we start from Equation B and the procedure is shown in Equation B.1.

$$R_4 = \frac{20}{8*15}R_3 \tag{A.1}$$
$$R_4 \approx 1.7K\Omega$$

In this case it was necessary to find the closest and highest commercial resistance value to ensure that the signal at the input to the Arduino board did not take negative values. For that reason, $R_4 = 1.8K\Omega$.

$$(\frac{R_2}{R_1+R_2})(\frac{11600}{10000}) = \frac{5}{8} \tag{B.1}$$
$$\frac{R_2}{R_1+R_2} = 0.538$$
$$R_2 - 0.538R_2 = 0.538R_1$$
$$R_1 \approx 8.6K\Omega$$

In Figure 3.6(a) we can see the circuit with the resistance values previously calculated and in Figure 3.6(b) the implementation in an experimental board to ensure the highest precision in the measured values.

Once the circuit was implemented, it was necessary to perform the measurements

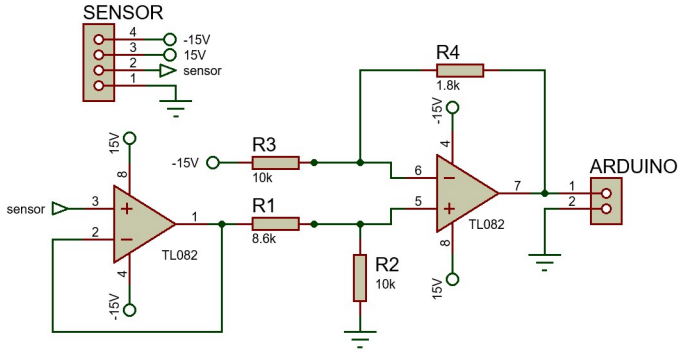

(a) Signal Conditioning Circuit Schematic.

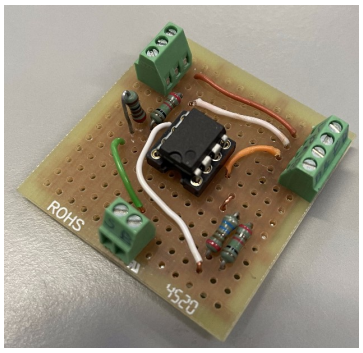

(b) SCC Board.

Figure 3.6: Implemented Circuit.

again to ensure that the signal output values showed a behavior within the ranges for which the SCC was designed. In the first instance, it was carried out in a limited range of values, the results are shown in Figure 3.7 being able to observe that the linear behavior is maintained and that the result obtained is very close to the expected one.

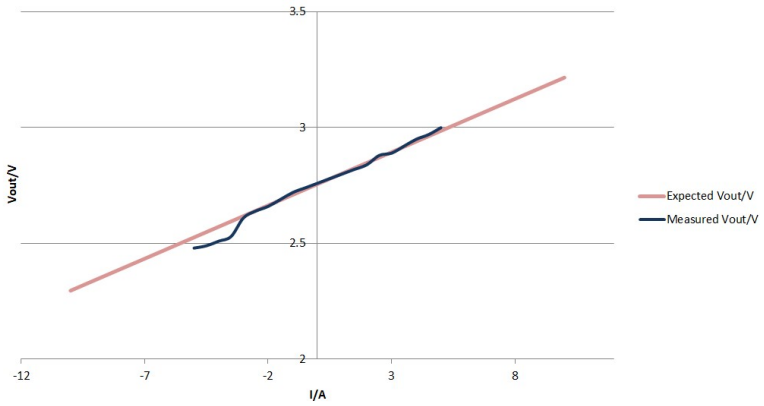

Figure 3.7: Measurements for SCC V.1.

However, due to the double power supply that is required to power the sensor, the signal presents a lot of noise, which makes it difficult to process it for the subsequent RMS current calculation since the reading by the Arduino varies a lot with the noise present at its input as shown in Figure 3.8. The yellow signal corresponds to the signal at the sensor output and was measured using a scale of $0.2V/div$. The light blue signal corresponds to the signal read by the Arduino board and it was measured using a scale of $1V/div$. It

can be seen that it is necessary to redesign the previous circuit, so this procedure will be shown in Section 3.2.

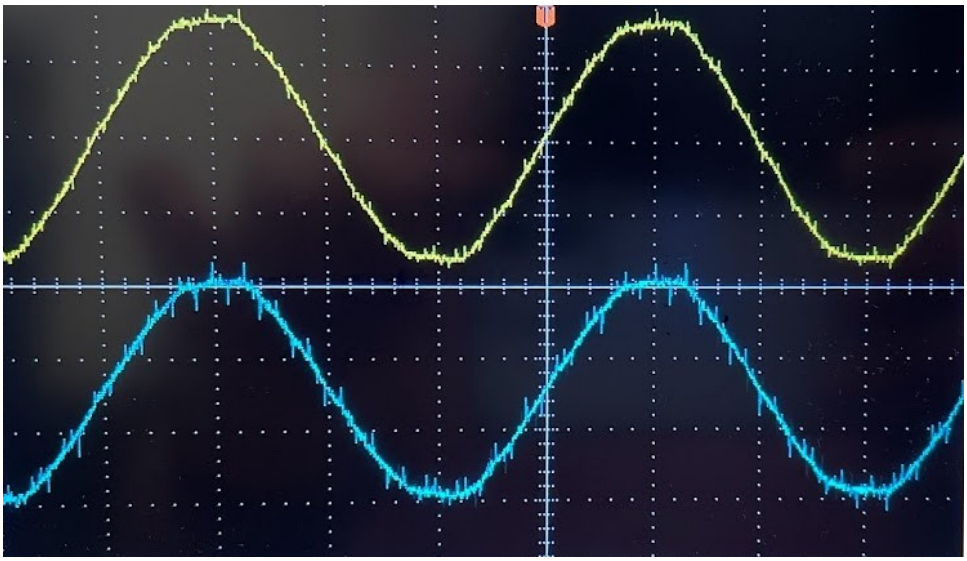

Figure 3.8: Noise in Signal Present Due to Double Power Supply.

3.1.3 Sensor Calibration

Since the variation or expected output for a given current value is not specified in the datasheet, it was necessary to measure such output and its behavior in the face of current variations. In a first instance, the behavior of the HST023R sensor with direct current was measured because the source available at that time delivered that type of current, also because the main objective at that time was to know the behavior of the sensor. It can be seen a linear behavior in the range reached in a first instance, as it is shown in Figure 3.9. At the same time, the signal at the output of the signal conditioner circuit designed to be able to connect said output to the analog inputs of the Arduino was measured and thus be able to process the information by software for the subsequent calculation of the I_{RMS}.

In Figure 3.10 we can see the graph that compares the values measured with the expected values of V_{out}. Both showing a practically linear behavior and with very little difference between the two values, observing a Standard Error (SE) $SE = 0.0495$.

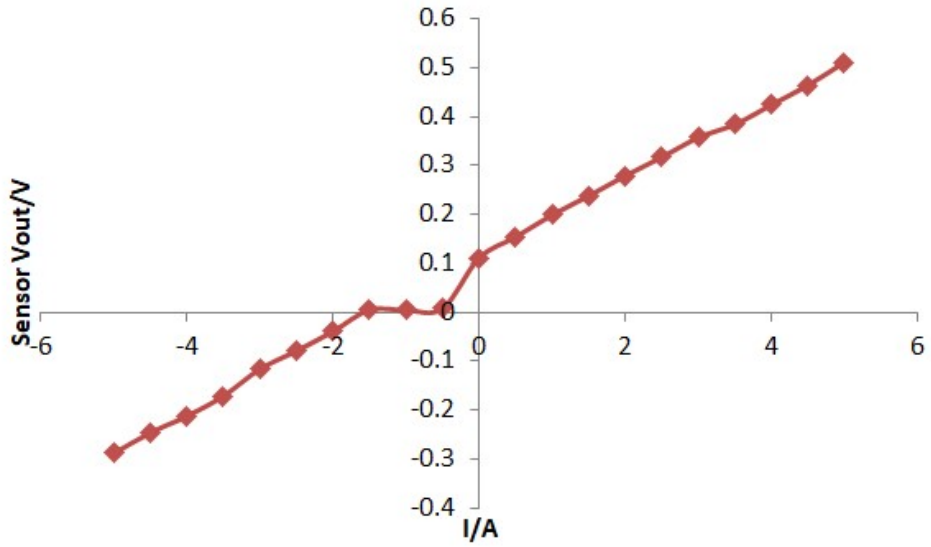

Figure 3.9: Sensor First Test Measurements.

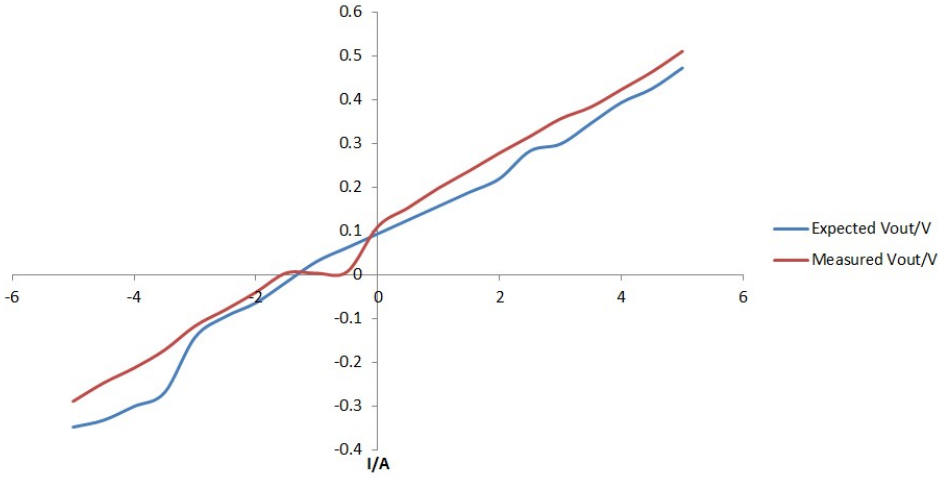

Figure 3.10: Expected Vout vs. Measured Vout.

3.2 Signal conditioning circuit V.2

As mentioned in the previous section, due to the noise present in the signal it was necessary to design a new SCC adding capacitors to be able to reject frequencies that are outside the band (50Hz), and at the same time it was used to increase the guarantee that the signal remained within the necessary levels. The new circuit is shown in Figure 3.11.

In this case, our reference voltage will be $V1$, and we will call the signal received from

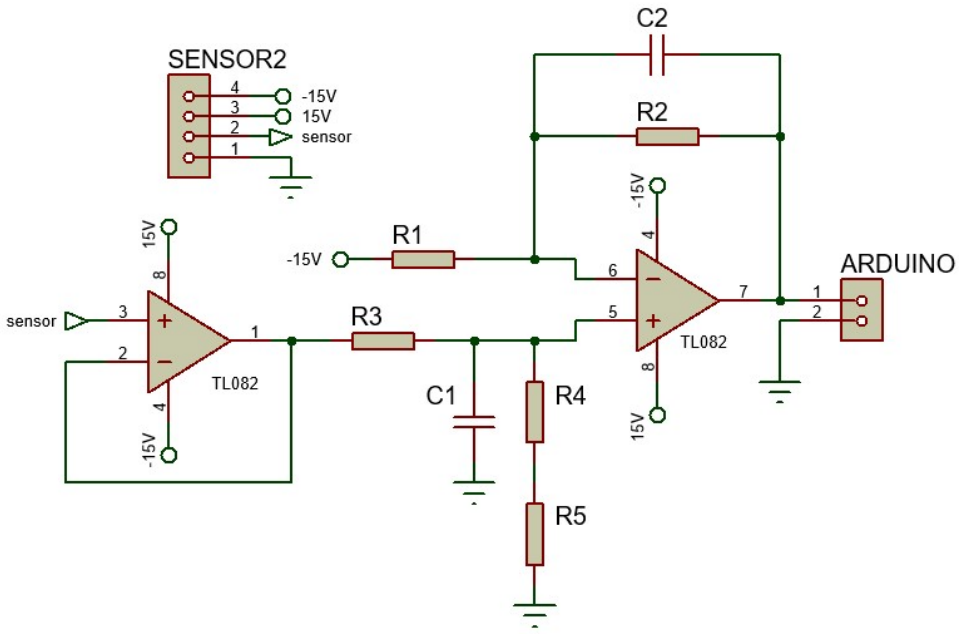

Figure 3.11: Differential Amplifier V.2.

the sensor $V2$.

The value of V_{out} is defined by Equation 3.8 and Equation 3.9, the last one corresponding to the redefinition of its limits since it is decided to work with the ESP32 board, these limits are shown in Figure 3.12.

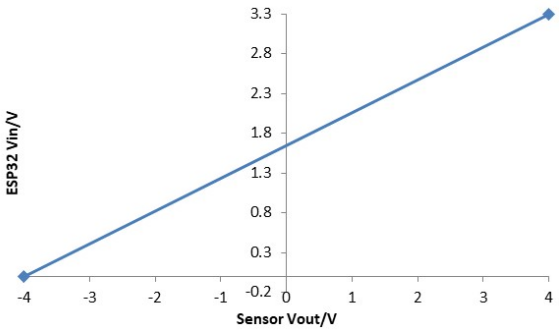

Figure 3.12: Relation between Vout and the possible input values of the ESP32 board.

$$V_{out} = (\frac{R_4}{R_3 + R_4})(\frac{R_2 + R_1}{R_1})V2 - \frac{R_2}{R_1}V1 \tag{3.8}$$

$$V_{out} = \frac{3}{8}V2 + 1.8 \tag{3.9}$$

Equating the Equation 3.8 with 3.9 we can obtain the following correlations:

$$-\frac{R_2}{R_1}V1 = 1.8 \tag{3.10}$$

$$(\frac{R_4}{R_3 + R_4})(\frac{R_2 + R_1}{R_1}) = \frac{3}{8} \tag{3.11}$$

Where $V1 = -15V$, then we have:

$$\frac{R_2}{R_1} = \frac{1.8}{15} \tag{3.12}$$

$$(\frac{R_4}{R_3 + R_4})(\frac{1.8}{15 + 1}) = \frac{3}{8} \tag{3.13}$$

$$\frac{R_3}{R_4} = \frac{149}{75} \tag{3.14}$$

To guarantee the input impedance condition $R_3 + R_4 > 10K\Omega$, therefore the values of the resistors would be:

Parameter	**Value**
R_1	$10K\Omega$
R_2	$1.2K\Omega$
R_3	$22K\Omega$
R_4	$11K\Omega$

Table 3.2: Calculated Values of Resistances.

In Figure 3.13(a) we can see the circuit with the resistance values previously calculated and in Figure 3.13(b) the implementation in an experimental board to ensure the highest precision in the measured values.

Once the circuit was implemented, it was also necessary to perform the measurements again to ensure that the signal output values showed a behavior within the ranges for

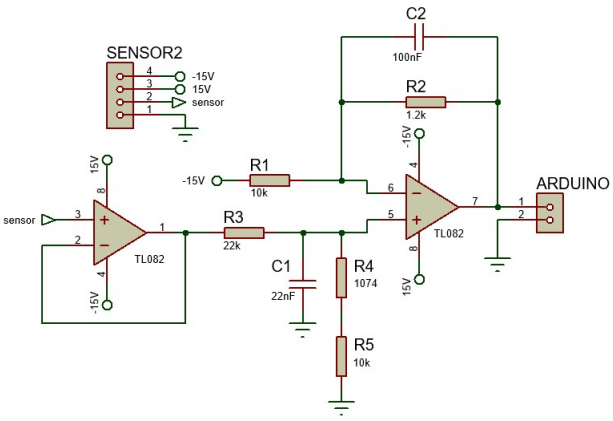

(a) Signal Conditioning Circuit Schematic V2.

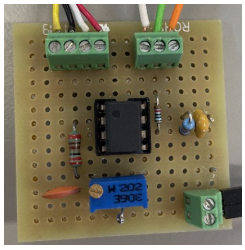

(b) SCC V2 board.

Figure 3.13: Implemented circuit.

which the SCC V2 was designed. The results are shown in Figure 3.14 and we can see also a linear behavior.

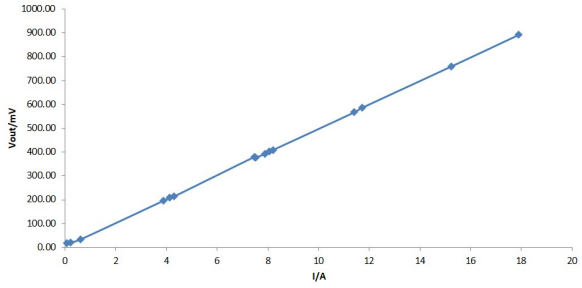

Figure 3.14: Measurements for SCC V.2.

In this case, it can be seen in the Figure 3.15 that the signal that is read by the Arduino board has less noise than in the previous case. As in the previous section, the yellow signal corresponds to the signal at the sensor output and was measured using a scale of $0.1V/div$. The light blue signal corresponds to the signal read by the Arduino board and it was measured using a scale of $1V/div$.

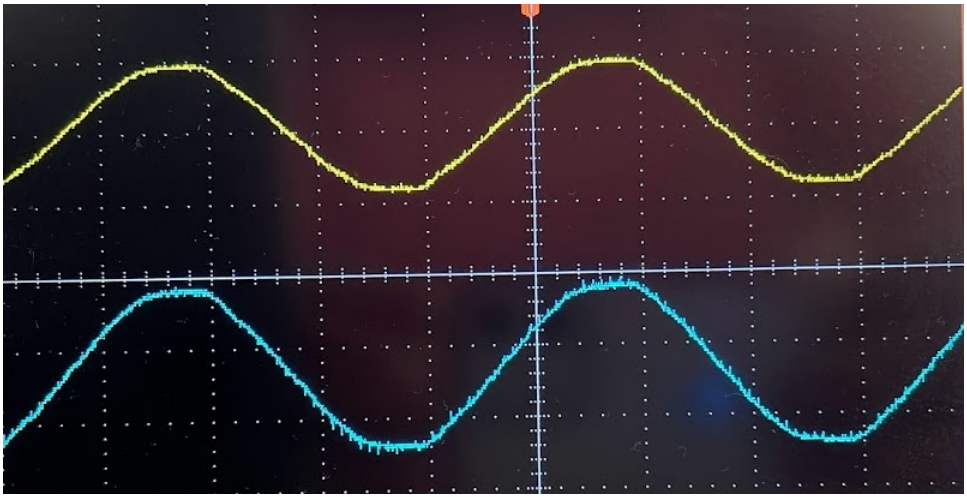

Figure 3.15: Noise in Signal Present Due to Double Power Supply.

3.3 Design of a Digital Filter

Despite having obtained good results, it was still necessary to make a digital filter not only to ensure the measurement of values that were within the measured frequency band, in this case the 50Hz corresponding to the mains frequency, but also because the sensor HST023R presents a small offset value at its output, which translates into an error in the calculation of I_{RMS}.

There are several possible options that are needed to test:

- Analog filtering;
- Digital filtering:
  - Inverse NOTCH filter to ensure that only the 50Hz component is caught. This eliminates the mean value of the signal and ensures that high-frequency fluctuations are attenuated.
  - Low pass filter. In this case, it is possible to set a higher bandwidth in order to cover a wider spectrum of the input signal. For example up to 100Hz.

For this project, it was decided to design an inverse Notch filter using the "Filter Design" tool of Matlab with the following characteristics:

- Frequency peak: 50Hz (desired frequency).
- Sampling rate: 1kHz.
- Bandwidth: 1Hz.

Figure 3.3 shows the frequency response for the digital filter.

This filter removes the mean value of the signal and ensures that high frequency fluctuations are attenuated. The transfer function in the z domain is shown in Equation 3.15.

$$H(z) = 0.00614\frac{1 - z^{-2}}{1 - 1.89z^{-1} + 0.988z^{-2}} \tag{3.15}$$

Being the difference equation the one that is effectively implemented in the microcontroller and that is shown in Equation 3.16, where $y(n)$ and $\mu(n)$ refer to the samples present at the filter output and input, respectively, at time nT. Here, n refers to an integer designating the sample number and T to the sampling period which, in this case, is equal to $1ms$.

$$y(n) = 1.89y(n-1) - 0.988y(n-2) + 0.00614[\mu(n) - \mu(n-2)] \tag{3.16}$$

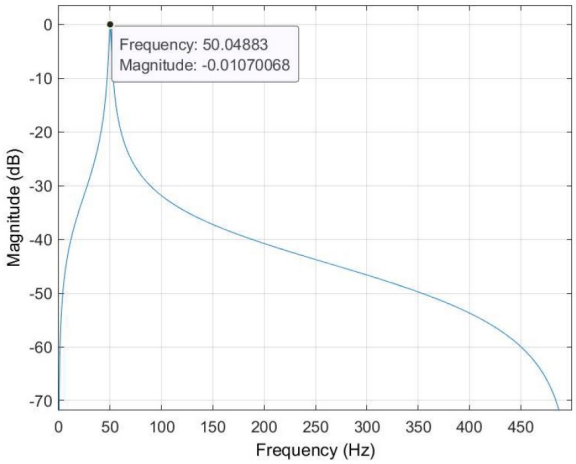

Figure 3.16: Frequency Response of the Inverse Notch Filter.

3.4 Final Measurements

In this section, the two experiments that were carried out for said sensor will be presented: in Section 3.4.1 the results obtained for the Arduino board will be presented and in Section 3.4.2 the results obtained with the ESP32 board.

3.4.1 Results with Arduino

Once the filter was calculated and implemented in our Arduino code, we were finally able to perform the last measurements required to obtain the equation that determines the behavior of our sensor when measuring a certain current value (I), with respect to the readings obtained at the Arduino's digital input (M). The first results are shown in the graph of Figure 3.17 and said equation is shown in Equation 3.17.

$$I = 0.4012 * M \tag{3.17}$$

In practice, it was necessary to force the intersection of the line to zero since that helped the error to decrease a few decimal places.

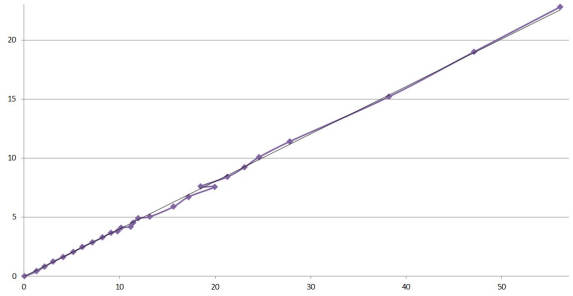

Figure 3.17: Behavior of the signal with Arduino.

Once the equation is obtained, it is added to the Arduino code to finally obtain the value of the effective current measured by the HST023R sensor. Some measurements were made with different and also known values of currents, obtaining an error of approximately **0.88%**. A good result since we are able to measure currents less than 1A, which many of the commercial sensors can not measure.

3.4.2 Results with ESP32

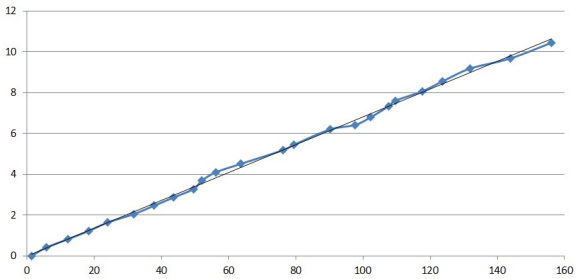

Figure 3.18: Behavior of the signal with ESP32.

A very similar study was made with the ESP32 board, the results of the measurements to determine the transfer function are shown in Figure 3.18, here it was also necessary to force the intersection of the line to zero. The equation that determines the behavior of our sensor when measuring a certain current value (I), with respect to the readings obtained at the ESP32's digital input (M) for this case, is expressed in Equation 3.18.

$$I = 0.0682 * M \tag{3.18}$$

In this experiment, known currents were also measured once the code was modified. In this case, the error in measurements is approximately **0.67%**, it is still a very good result and we are also capable of measuring currents below 1A.

3.5 Custom Current Sensor

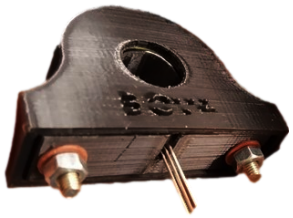

Figure 3.19: Current Sensor With SS49E.

Despite having obtained very good results with the HST023R sensor, when designing

a node, the fact of needing a double power supply makes the node impractical, whether that source was external or included in the design. In addition, it must be taken into account that designing a system whose components require different power supply values means that there is a lot of energy dissipation in the form of heat. This is due to the fact that DC-DC converters have an efficiency of approximately 80%, that is, the remaining 20% is energy that is not used, but is dissipated. That is why it was finally decided to design a current sensor with the SS49E hall effect sensor and a toroid, which allows the measurement of electrical currents up to 40A.

Although there are several ways to measure the value of the electric current, for example using a Rogowsky coil, it was considered for the IoT node to be developed the use of a Hall effect sensor built into a primary element, which in this case is a toroid made of ferromagnetic material (iron pentacarbonyl). The Hall effect sensor is a device that generates a voltage proportional to the intensity of the magnetic field that passes through it and will be located inside the primary element as shown in Figure 3.20. In this figure, an electrical conductor can be seen, carried by a current. electric $i(t)$ passing through the primary element. This electric current generates, at a point in the space around the conductor, a magnetic field whose intensity is proportional to the intensity of the electric current. The primary element works as a magnetic lens focusing the magnetic field and forcing it to pass through the Hall effect sensor which, as it can be seen, is built into the toroid.

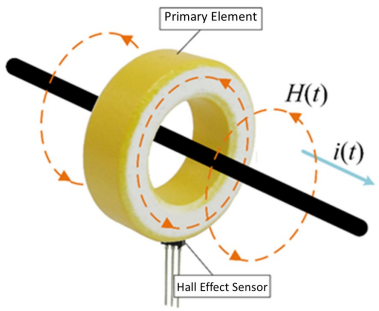

Figure 3.20: Configuration Involving a Toroid as a Primary Element.

SS49E Linear Hall-effect sensor is small, versatile linear Hall-effect device that is operated by the magnetic field from a permanent magnet or an electromagnet. The linear sourcing output voltage is set by the supply voltage and varies in proportion to the strength of the magnetic field. The integrated circuitry features low noise output, which makes it unnecessary to use external filtering [23].

The electrical and performance characteristics can be seen in Appendix A.

3.5.1 Custom Current Sensor Construction

The SS49E hall effect sensor was integrated into a toroid and a PLA encapsulation was also created to give it mechanical robustness. Figure 3.21(a) shows the three-dimensional model created in SolidWorks® that was used to generate the Computer Numerical Control (CNC) code used by the 3D printer. Figure 3.21(b) shows the 3D printing process performed on an Ender 3® machine using PLA as filament.

(a) 3D Design of the Current Sensor Package.

(b) Detail of the 3D Printing Process Using PLA.

Figure 3.21: Custom Current Sensor.

The final result of the current sensor construction procedure is shown in Figure 3.22. The cut in the toroid was made using an abrasive disk and the sensor was attached to this groove using two-component epoxy glue.

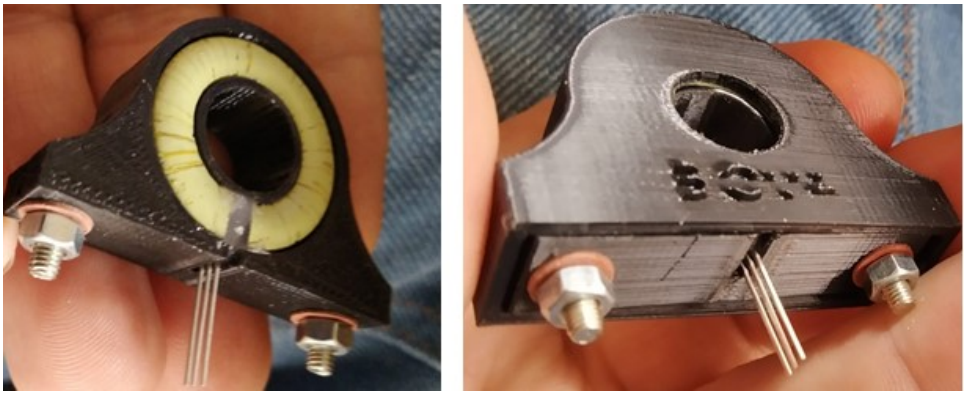

Figure 3.22: Final Result of Creating the Custom Current Sensor for BIOMA.

3.5.2 Sensor Calibration

As in the case of the previous current sensor, it was also necessary to study the behavior of the SS49E sensor against current variations. This process involved performing a sequence of tests where different values of electrical current were injected into an electrical conductor that passed through the toroid and the voltage values at the sensor output were recorded (Figure 3.23). As in the previous case, it was possible to carry out the measurement in a restricted current range, the maximum reached being 18A.

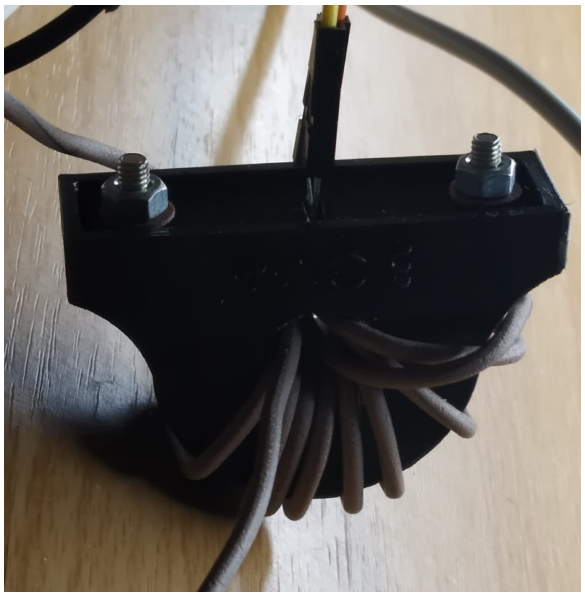

Figure 3.23: Measurement Method for Custom Current Sensor Calibration.

Figure 3.24 shows the graph of the results obtained, where we can also observe a linear behavior in the tested range. Assuming that the sensor saturates for values around 80% of the supply voltage, it is expected that this device will be capable of measuring currents that can reach up to 50A.

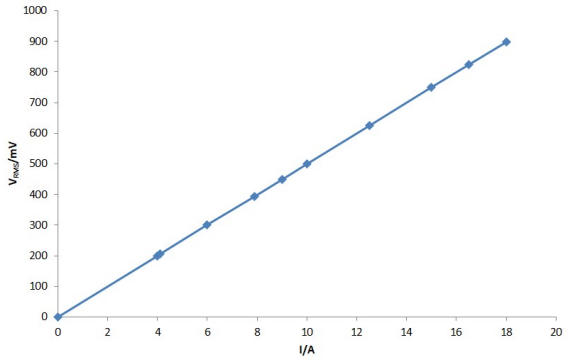

Figure 3.24: Custom Current Sensor Calibration Curve.

The fact that this Hall effect sensor has shown greater linearity in its results, compared with the previous one, may be due to the fact that, as it was not possible to manufacture it as an open loop sensor like the first one, its characteristics are more linear. Or perhaps it could also be due to the microcontroller used to carry out the tests and the implemented code, so that in future work some of these hypotheses would have to be verified.

Chapter 4

The System Development

This chapter analyzes the steps for the development of the final work. Starting with Section 4.1 where the general description of the electronic architecture of the system will be provided, followed by Section 4.2, which will show the development of the system firmware.

4.1 Hardware Development

For the development of the Printed Circuit Board (PCB), the online tool EasyEDA was used to be able to order its subsequent printing.

The overview of the electronic architecture of the system is based on three modules responsible for maintaining its operation. As shown in Figure 4.1 these modules are divided into: current sensor, which was discussed in Section 3.5, microcontroller, and power supply.

In the case of the microcontroller module, it is made up of the ATtiny85 and the RFM95 LoRa transceiver. The power module is made up of a battery, battery management circuit and a DC-DC buck converter, responsible for reducing the voltage.

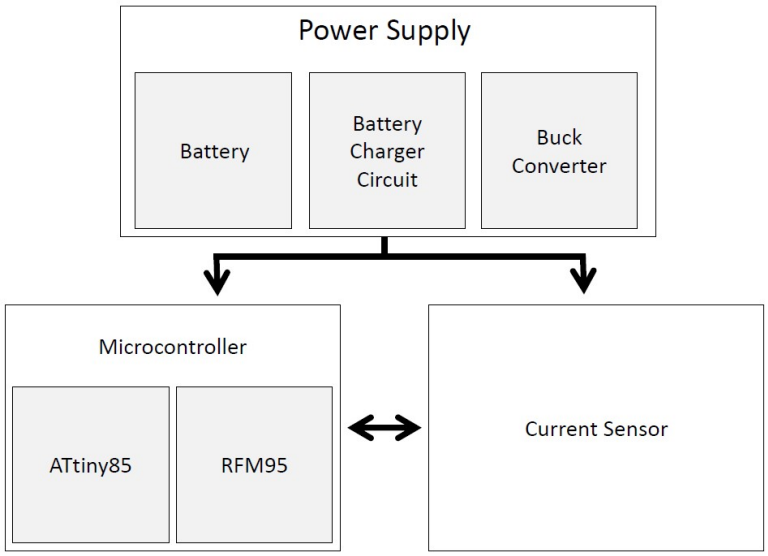

Figure 4.1: Modules of the Electronic Architecture.

4.1.1 Microcontroller Module

This module is composed of the ATtiny85 microcontroller and the RFM95 LoRa transceiver. Both communicate with each other via Serial Peripheral Interface (SPI).

The USI three-wire mode is compliant to the SPI mode 0 and 1, but does not have the slave select (SS) pin functionality. However, this feature can be implemented in software, if required. Pin names used in this mode are DI, DO, and USCK. A simplified block diagram of the USI is shown in Figure 4.2 [24].

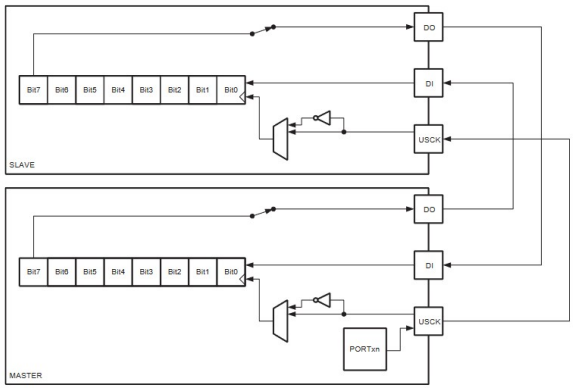

Figure 4.2: Three-wire Mode Operation, Simplified Diagram.
Source: [24].

With that in mind the connections between the microcontroller and the RFM95 are shown in Figure 4.3, in turn some pins were added for programming the ATtiny85 and thus not limit the node to only one type of use and to be able to change the functionalities of the code when necessary.

The program used to send LoRa packets through the RFM95 module is shown in Appendix B.

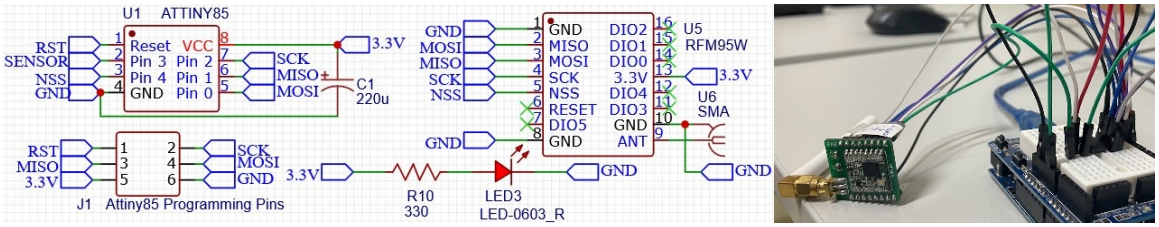

Figure 4.3: ATtiny85 and RFM95 Connections.

4.1.2 Power Supply Module

As mentioned above, the power supply module is composed by the battery, the battery management circuit and the DC-DC buck converter. The battery used for this work is the ICR18650-26FM model, with a nominal capacity energy of 1351-2199mAh and a nominal voltage during the whole discharge process of 3.7V.

Since a lithium-ion battery cell is used, a Battery Management System (BMS) needs to be taken in order to enhance safety characteristics [25] and since this node is intended to be installed in a supply chain and to work independently, it is also necessary to add a circuit that allows the built-in battery to be charged whenever necessary. In this work is used the TP4056 module (see Figure 4.4), which is made for charging lithium batteries using constant current and constant voltage, besides, the module provides necessary protection for the batteries such as overdischarge/overcharge protection, overcurrent and short-circuit protection, soft start protection to limit inrush current and trickle charge for battery reconditioning.

The integrated circuit responsible for the constant-current/constant-voltage linear

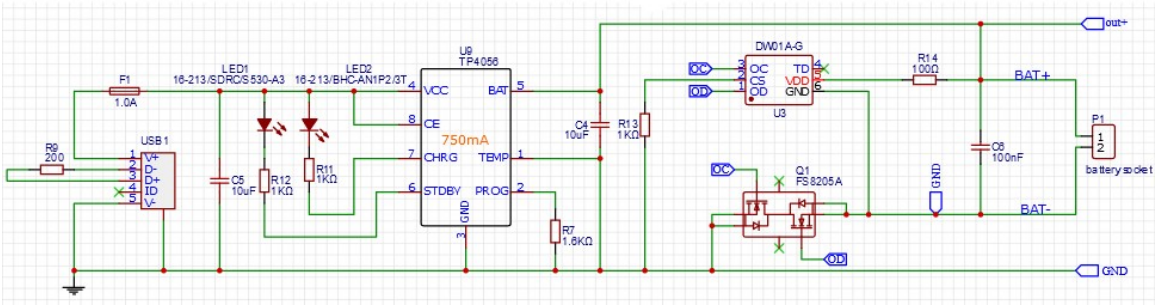

Figure 4.4: Battery Management Schematic Circuit.

charger is the TP4056 integrated circuit and it includes several features such as current monitor, under voltage lockout, automatic recharge and two status pin, to indicate charge termination and presence of an input voltage [26]. At the same time, The DW01A and the FS8205A work together in order to protect the battery from damage or degrading the lifetime due to overcharge, overdischarge, and/or overcurrent [27], [28].

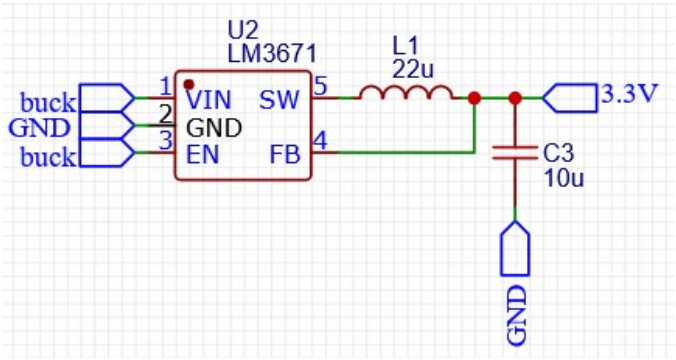

Figure 4.5: Converter Schematic Circuit.

On the other hand, the ATtiny85, RFM95 LoRa module and the current sensor can be powered at 3.3V. As mentioned earlier, the battery has the peculiarity of offering 3.7V, so it was necessary to add the buck circuit and thus reduce the voltage to the optimum for these components. This circuit is shown in Figure 4.5.

According to its datasheet, the ATtiny85 has a idle supply current approximately equal to $0.068mA$ and an active supply current approximately equal to $0.12mA$. The RFM95 LoRa Module has a supply current in standby mode approximately equal to $1.6mA$ and an active supply current in transmit mode that varies between $20 - 120mA$, however, being

programmed to transmit only once per hour, this consumption does not imply a great factor when calculating the average consumption of the circuit, so it will not be considered in the calculation of the battery autonomy. For the case of the current sensor, the SS49E has a typical consumption of $4.2mA$. All of this data can be seen in Appendix A.

Theoretically, the battery would have an autonomy of $878.4h$, which would translate into approximately 36 and a half days, assuming that the current sensor works 24 hours a day without stopping. In future work it would be important to carry out the autonomy test under different circumstances and check if the value obtained theoretically is close to the real value.

4.1.3 Electronic Circuit Schematic

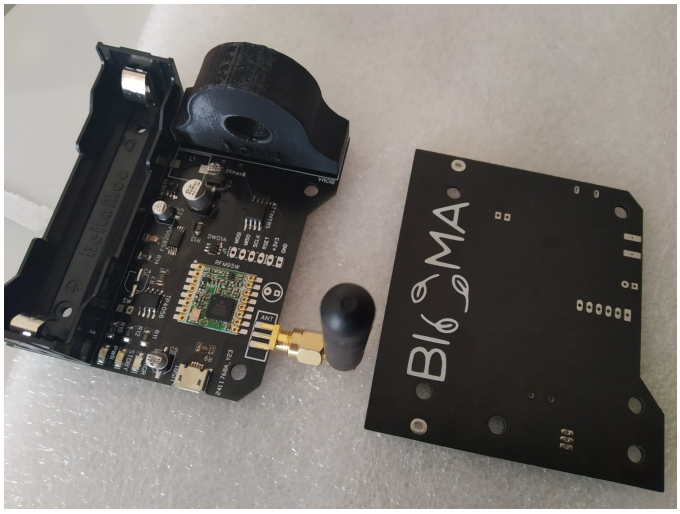

Figure 4.6: Printed Circuit Board.

In addition to the aforementioned, a jumper was added to be able to disconnect the system from the battery (turn it off), so the final circuit schematic for this first prototype is shown in Figure 4.8 and the PCB layout in Figure 4.6.

Initially, the PCB had been designed with the idea of soldering its components in a reflow oven, however it was not possible to obtain it within a short period of time, so a stencil had to be designed using a digital tool, to then print it in 3D and proceed with the

soldering process. Both the stencil and the soldering process can be seen in Figures 4.7(a) and 4.7(b) respectively.

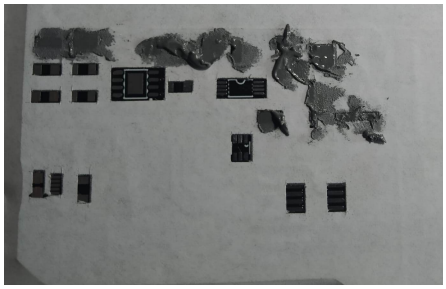

(a) Stencil used for soldering.

(b) Microscope used to help in soldering process.

Figure 4.7: Soldering Process.

4.2 Firmware Development

This section describes how the acquisition and processing of the signal coming from the current sensor is done. As mentioned previously, the purpose of the node is to measure the electrical current consumed by a certain device with single-phase power. This implies that the signal at the sensor output will have a sinusoidal waveform with a frequency of $50Hz$ and an amplitude that will depend on the intensity of the electrical current that runs through the electrical conductor under measurement.

It is then necessary to define the rest of the signal processing stages involved in the transformation of the signal coming from the sensor. All these steps will be performed by a single controller, in this case the ATtiny85. Said microcontroller will be responsible for:

- Conversion of the signal from the analog domain to the digital domain, performed by the 10-bit A/D converter included in the microcontroller.
- Digital filtering to remove the effect of high frequency disturbances as well as offset DC voltages.
- Numerical calculation of the RMS current.

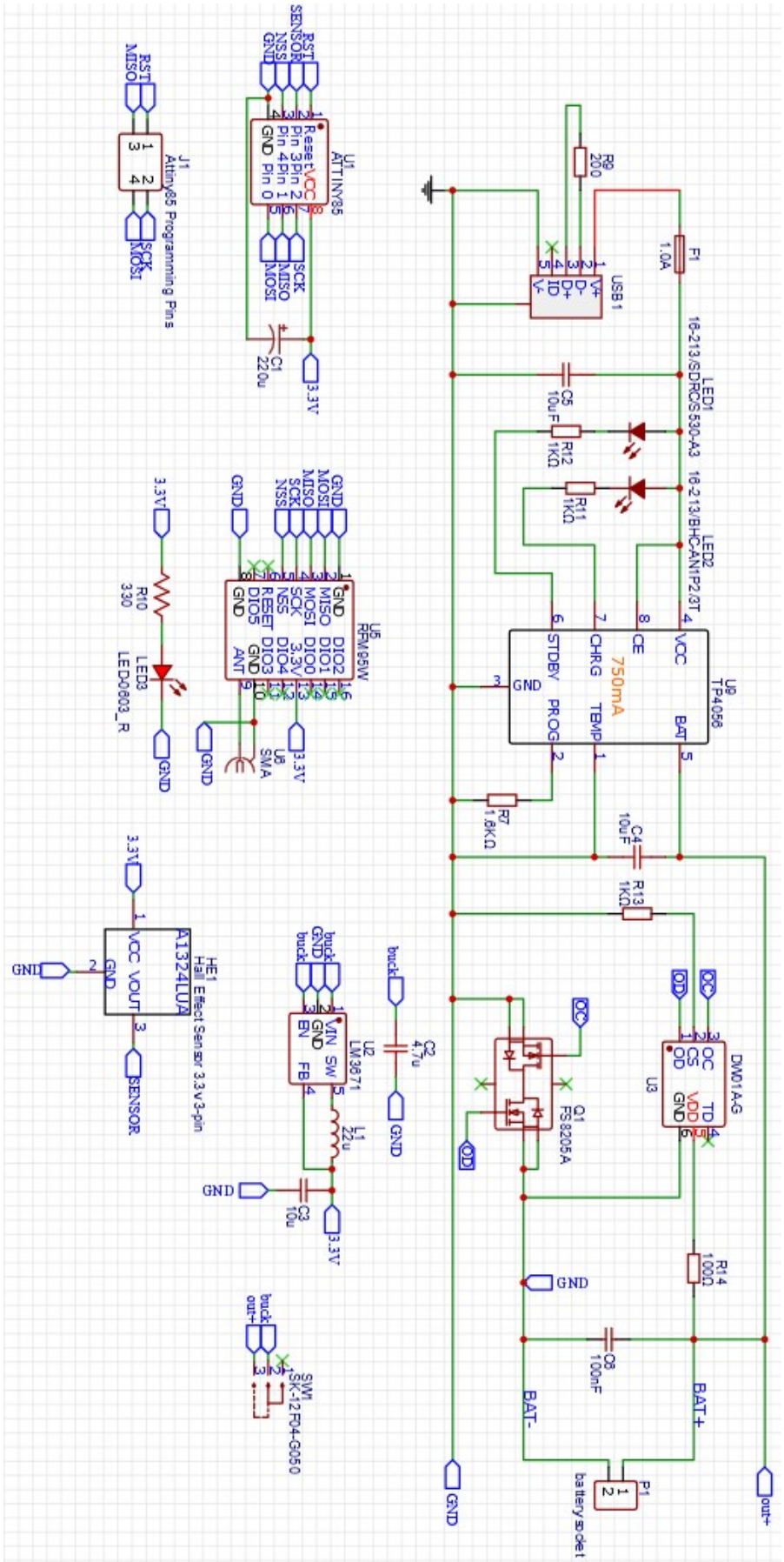
U1
ATTINY85
RST
SENSOR
NSS
GND
Reset/PB5
Pin 3/PB3
Pin 4/PB4
GND Pin 0
VCC
Pin 2/PB2
Pin 1/PB1
SCK
MISO
MOSI
C1
220u
3.3V
J1
Attiny85 Programming Pins
RST
MISO
SCK
MOSI
U5
RFM95W
GND
MOSI
MISO
SCK
NSS
DIO2
DIO1
DIO0
3.3V
DIO4
DIO3
GND
ANT
RESET
DIO5
U6
SMA
R10
330
LED3
LED-0603_R
HE1
Hall Effect Sensor 3.3v 3-pin
A1324LUA
VCC
VOUT
GND
SENSOR
U2
LM3671
VIN
SW
GND
EN
FB
L1
22u
C2
4.7u
C3
10u
buck
out+
SW1
SK-12F04-G050
U8
TP4056
CE
VCC
CHRG
STDBY
GND
PROG
TEMP
BAT
750mA
LED1
16-213/SDRGVS30-A3
LED2
16-213/BHCANYP2/3T
R9
200
USB1
V+
D-
D+
ID
V-
F1
1.0A
C5
10uF
R12
1KΩ
R11
1KΩ
R7
1.8KΩ
C4
10uF
R13
1KΩ
U3
DW01A-G
OC
CS
OD
TD
VDD
GND
Q1
FS8205A
R14
100Ω
C8
100nF
BAT+
BAT-
P1
battery socket
out+
GND

- Sending the information to the LoRa module.

Figure 4.9 shows the flowchart that represents the operations for which the microcontroller was programmed.

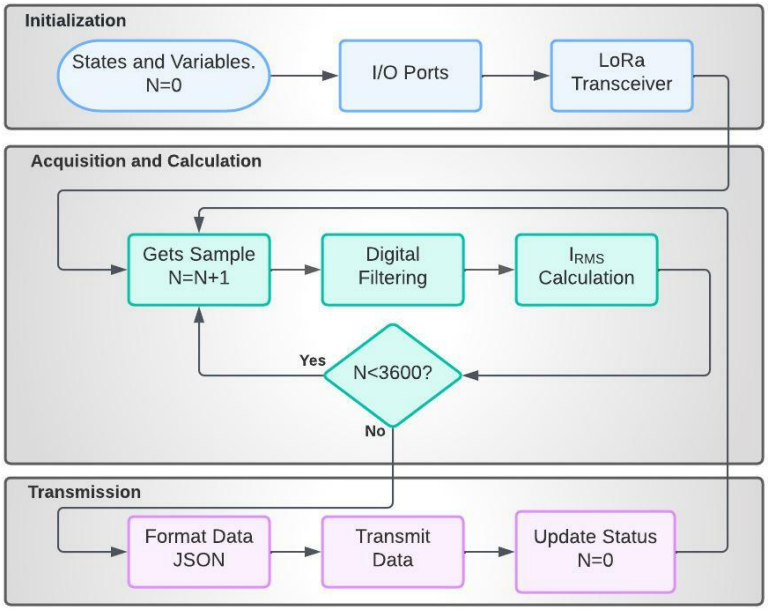

Figure 4.9: Flowchart Related to the Firmware Operation Running on the Microcontroller.

When the IoT node is connected, the microcontroller initializes the state variables, the I/O ports as well as the LoRa transceiver configuration. After finishing the initialization process, the data acquisition and I_{RMS} calculation stage begins, where the IoT node measures the value of the electrical energy consumed by a certain device during a period of time of one hour. This value is calculated from the signal generated by the current sensor that is acquired through periodic sampling using a rate of 1000 samples per second. Every hour, the calculated value is encapsulated in a JavaScript Object Notation (JSON) payload and sent to a FIWARE context manager.

JSON is a standard text format for storing and transmitting data over a network. Application Programming Interface (API) clients use this format to send or receive data from the server. It represents four primitive types: strings, numbers, boolean values, and

null; and two structured types: objects and arrays.

4.2.1 Method for RMS Current Calculation for Final Node

In this case, the waveform of the signal at the sensor output corresponds to a sinusoidal wave with a frequency equal to 50Hz and whose amplitude depends on the amplitude of the electrical current that runs through the electrical conductor being measured, as we will see in Section 3.5.2. In the exponential weighting method, I_{RMS} is computed recursively using the following expressions:

$$I_{RMS}(n) = \sqrt{(1 - \frac{1}{w_n})I^2_{RMS}(n-1) + \frac{1}{w_k}i^2(k)} \tag{4.1}$$

$$w_n = \lambda w_{n-1} + 1 \tag{4.2}$$

Where $I_{RMS}(n)$ refers to the effective value of the current measured at instant nT, $i(n)$ is the instantaneous value of the current present, w_n is the weight applied to the current sample and $0 \leq \lambda \leq 1$ is called the forgetting factor. Note that, for the initial sample $n = 0$ and $w_0 = 1$.

An analysis of the behavior of this algorithm was carried out together with the sliding window methods and the incremental method. Based on a result of 1000 trials, the average execution time was $0.65ns$, from a relative point of view, it is 14 times faster than the sliding window method.

In addition to the execution time, another great advantage found for the weighted exponential method compared to the other two is that it does not consume much memory of the microcontroller, being of great benefit in the case of the ATtiny85, since this one has 512 SRAM.

Figure 4.10 shows the flow chart that will help to better understand the process performed internally by the microcontroller. The implemented code can be seen in Appendix B.

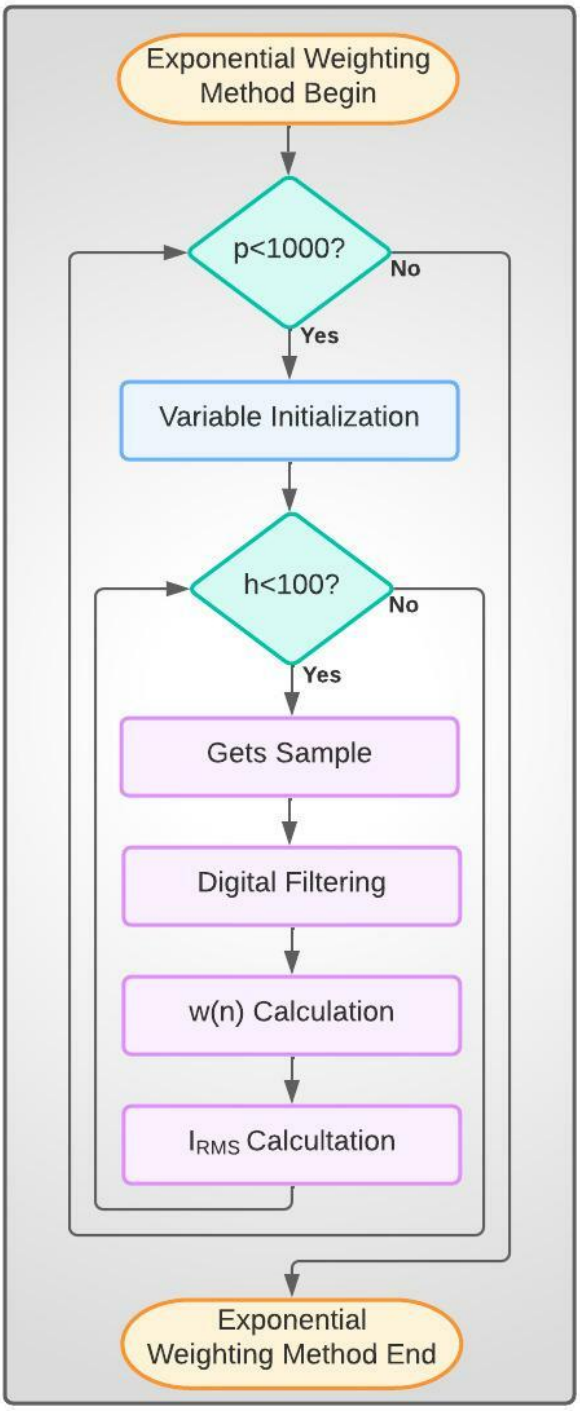

Figure 4.10: Flowchart Related to the RMS Current Calculation Running on the Microcontroller.

Chapter 5

Results and Discussions

This chapter presents some overall considerations on the solution adopted for the reading of electric current in Section 5.1, followed by Section 5.2 it is provided the price list of the electronic components used .

5.1 Overall Considerations

In this section, some basic considerations about the solution adopted for reading the electrical current consumption will be presented.

Any device whose purpose is to be part of an IoT application must be connected to a network at all times, otherwise the system will not be able to update the data in the database. In the case of not having an internet connection, some modifications could be made in the ATtiny85 configuration to save the results of the measurements carried out, although it must be taken into account that this microcontroller has a limited and relatively small memory size. However, this would only be applicable if it was not necessary to work with real-time data.

The communication protocol developed in this work does not use any API protection. This means that APIs may be subject to additional security threats and vulnerabilities. Therefore, the use of some type of encryption would be interesting to address security considerations.

Another point to consider when installing the system is the environment in which the device will be placed. Which makes it necessary to first check if the environment will be aggressive for the equipment and if the measurements will be affected over time.

5.2 System Cost and Architecture Proposal

This section will provide a generalized description of the price of the materials used in the development of the final LoRa node. In the case of the components that are part of the PCB, they will not be considered separately but will be included in the total, except for the RFM95 module, the ATtiny85 and the battery.

Items	**Price (€)**
RFM95 + Antenna	4.66
ATtiny85	0.084
PCB + components	3
Battery	2.42
Total	**10,16**

Table 5.1: Approximate price table of electronic components used. *Prices based on Aliexpress (February, 2022).*

From Table 5.1, it can be seen that the developed system provides a low-cost IoT solution, with prices ranging between 10 and 11 €, considering that they are based on the search on a single website.

Another clarification regarding this price list is that the toroid was not included because it was reused for this prototype. In case it is needed to buy one, the price varies between 1 and 4 €, depending on the material and size. PLA material is also not included in the calculation.

Having a low-cost device has an advantage in its scalability, since the application can be moved to different points and work in the same way in any of them, that is, in an independent way.

Chapter 6

Conclusions and Future Work

Currently, we are involved in the need not only to have an efficient and profitable production system, but also one that meets a certain standard of sustainability and efficient use of natural resources. In this context, the present work developed a solution based on IoT to be applied in any supply chain that wishes to monitor its energy consumption.

The advantage of IoT solutions is that they are economical, sustainable systems with high energy savings. As it was seen throughout the development of this work, it is possible to make a simple and compact node.

In general, there are several ways to measure electrical energy consumption, which represents an important indicator for the calculation of sustainability indicators. The measurement with a hall effect sensor integrated into a microcontroller proved to be satisfactory and affordable as part of the IoT solution for any type of supply chain. In addition to the measurement of electrical current, the solution developed here can serve as a basis for the development of sensors for the measurement of other parameters.

For future work, it is expected to implement encryption to the system since in this first phase the data does not present any level of security and therefore we cannot ensure the confidentiality of the data sent. Said encryption can be both at the node level, looking for an encryption supported by the ATtiny85 microcontroller, and/or at the broker from where the data will be accessed.

It is also important to study the robustness of this system, since we do not have a

certain guarantee that the data is not modified along the way, how many of the packets sent actually arrive and how many are lost; in addition to mounting several nodes simultaneously and studying whether or not there is a collision of packets.

The determination of repeatability, as well as other metrological quantities is also important, so it is necessary to replicate tests in various conditions (environmental and others) as well as the construction and testing of more sensors.

Another work that remains pending is to study its autonomy under different operating conditions and to measure the energy consumption of the whole node since they are important parameters when designing an IoT node.

Bibliography

[1] OECD, *Improving Energy Efficiency in the Agro-food Chain*. 2017, p. 108. DOI: https://doi.org/https://doi.org/10.1787/9789264278530-en. [Online]. Available: https://www.oecd-ilibrary.org/content/publication/9789264278530-en.

[2] D. Cemernek, H. Gursch, and R. Kern, "Big data as a promoter of industry 4.0: Lessons of the semiconductor industry," in *2017 IEEE 15th International Conference on Industrial Informatics (INDIN)*, 2017, pp. 239–244. DOI: 10.1109/INDIN.2017.8104778.

[3] J. Sen, S. Lee, Y. Choe, M. Lee, M. Domb, A. Pal, H. K. Rath, S. Shailendra, A. Bhattacharyya, A. Mihovska, M. Sarkar, H. Lee, M. Kim, and A. Averian, *Internet of Things: Technology, Applications and Standardization*. Aug. 2018.

[4] A. K. Jeretta Horn Nord and J. Paliszkiewicz, "The internet of things: Review and theoretical framework," *Expert Systems with Applications*, vol. 133, pp. 97–108, 2019.

[5] A. Huang, M. Huang, Z. Shao, X. Zhang, D. Wu, and C. Cao, "A practical marine wireless sensor network monitoring system based on lora and mqtt," in *2019 IEEE 2nd International Conference on Electronics Technology (ICET)*, 2019.

[6] Y.-W. Ma and J.-L. Chen, "Toward intelligent agriculture service platform with lora-based wireless sensor network," in *2018 IEEE International Conference on Applied System Invention (ICASI)*, 2018.

[7] L. Evers and P. Havinga, "Supply chain management automation using wireless sensor networks," in *2007 IEEE International Conference on Mobile Adhoc and Sensor Systems*, 2007.

[8] N. Wang and Z. Li, "Wireless sensor networks (wsns) in the agricultural and food industries," in. Dec. 2013, pp. 171–199.

[9] A. Tewari and B. Gupta, "Security, privacy and trust of different layers in internet-of-things (iots) framework," *Future Generation Computer Systems*, 2018.

[10] M. Thomas, P. Kumar, and V. Chandna, "Design, development, and commissioning of a supervisory control and data acquisition (scada) laboratory for research and training," *Power Systems, IEEE Transactions on*, vol. 19, pp. 1582–1588, Sep. 2004. DOI: 10.1109/TPWRS.2004.826770.

[11] T. Turc, "Ajax technology for internet of things," *Procedia Manufacturing*, vol. 32, pp. 613–618, 2019, 12th International Conference Interdisciplinarity in Engineering, INTER-ENG 2018, 4–5 October 2018, Tirgu Mures, Romania, ISSN: 2351-9789. DOI: https://doi.org/10.1016/j.promfg.2019.02.260.

[12] P. L. Wei Zhou Yuqing Zhang, "The effect of iot new features on security and privacy: New threats, existing solutions, and challenges yet to be solve," 2018.

[13] S. E. Ooi, R. Beuran, and Y. Tan, "Secure iot development: A maker's perspective," in *2021 IEEE International Conference on Omni-Layer Intelligent Systems (COINS)*, 2021. DOI: 10.1109/COINS51742.2021.9524205.

[14] C.-L. Tseng and F. J. Lin, "Extending scalability of iot/m2m platforms with fog computing," in *2018 IEEE 4th World Forum on Internet of Things (WF-IoT)*, 2018, pp. 825–830. DOI: 10.1109/WF-IoT.2018.8355143.

[15] S. Ziegler, "Considerations on ipv6 scalability for the internet of things — towards an intergalactic internet," in *2017 Global Internet of Things Summit (GIoTS)*, 2017. DOI: 10.1109/GIOTS.2017.8016238.

[16] *"iot edge developer survey report"*, Dec. 2021.

[17] P. Silventoinen and M. Kuisma, "Review on the current measurement systems in power electronics," Jan. 1999.

[18] H. Kirkham, "Current measurement methods for the smart grid," Aug. 2009. DOI: 10.1109/PES.2009.5275282.

[19] A. M. Patel, "Current measurement in power electronic and motor drive applications – a comprehensive study," M.S. thesis, University of Missouri-Rolla, 2007.

[20] G. E. Mog and E. P. Ribeiro, "Mean and rms calculations for sampled periodic signals with non-integer number of samples per period applied to ac energy systems,"

[21] T. Ngo, K. Min, and T. Vu, "Comparative study of fault detection methods based on time domain rms calculation," in *2019 IEEE Power Energy Society General Meeting (PESGM)*, 2019.

[22] J. M. F. Arias, M. O. Lopez, F. J. Q. Latorre, F. J. B. Outeiriño, and A. M. Muñoz, "A memory-efficient true-rms estimator in a limited-resources hardware," 2019.

[23] SEC, *SS49E Linear Hall Effect Sensor*, Datasheet.

[24] *Atmel 8-bit AVR Microcontroller with 2/4/8K Bytes In-System Programmable Flash*, Aug. 2013.

[25] M. K. G. (eds.), *Lithium-ion Battery Materials and Engineering: Current Topics and Problems from the Manufacturing Perspective*, 1st ed., ser. Green Energy and Technology. Springer-Verlag London, 2014, ISBN: 978-1-4471-6547-7.

[26] *Datasheet*, *1A Standalone Linear Li-Ion Battery Charger*, TP4056 Datasheet.

[27] *Datasheet*, *One Cell Lithium-ion/Polymer Battery Protection IC, Rev. 1.7*, DW01A DataSheet, May 2014.

[28] *Dual N-Channel Enhancement Mode Power MOSFET, Rev. 1.2*, FS8205A DataSheet, Aug. 2009.

[29] YHDC, *HST023R*, Datasheet.

[30] . HOPE MICROELECTRONICS CO. LTD, "RFM95/96/97/98(W) Low Power Range Transceiver Module V1.0," 2006.

[31] . Samsung SDI Co. LTD, *SPECIFICATION OF PRODUCT for Lithium-ion Rechargeable Cell Model : ICR18650-26F*, May 2009.

Appendix A

Technical data

This appendix shows the technical aspects of the components, such as datasheets and pinouts schemes.

I_{PN}	Rated input	±50A	±100A	±200A	±300A	±400A	±500A	±600A
Ipm	Input measurement range	±60A	±120A	±240A	±360A	±480A	±600A	±720A
Vout	Rated output	±4V						
X	Accuracy	1%						
εL	Linearity	1%						
Vc	Supply voltage	±12V/±15V						
Ic	Current consumption	≤±16mA						
Rl	Load impedance	≥10KΩ						
Voe	Zero offset voltage	≤±15mV						
Tr	Response time	≤5μs						
N.w	Weight	84g						
Ta	Operation temperature	-10～+70℃						
Ts	Storage temperature	-25～+70℃						
Bw	Band width	DC~25KHz						
Vd	Delectric strength	2.5KV 50Hz 1min						

Figure A.1: HST023R Electrical Parameters [29].

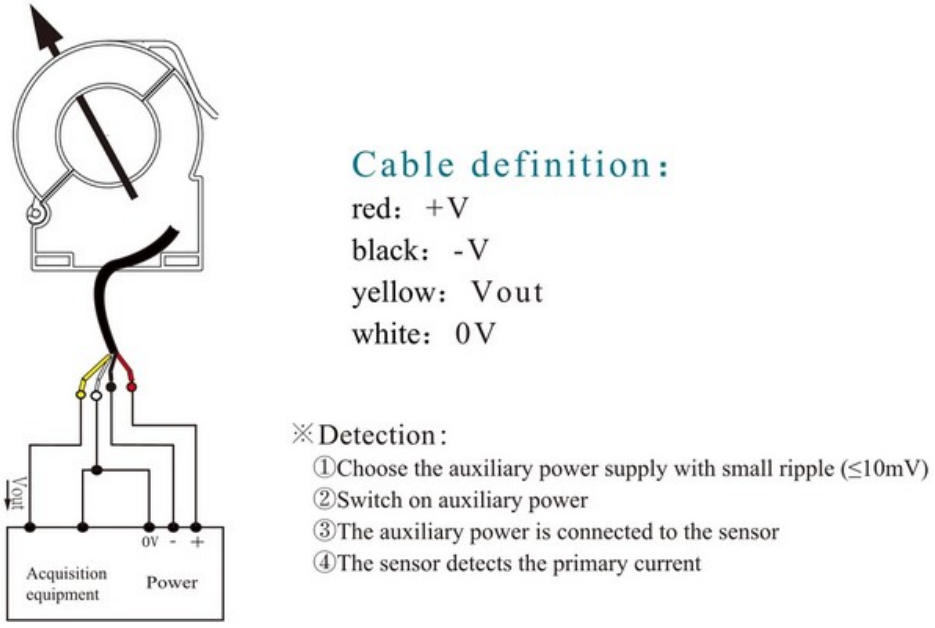

Figure A.2: HST023R Wiring Diagram [29].

Parameter	Symbol	Test Conditions	Min	Typ	Max	Units
Operating voltage	V_{CC}	Operating	3.0		6.5	V
Supply current	I_{CC}	Average		4.2	8.0	mA
Output Current	I_{OUT}		1.0	1.5		mA
Response Time	Tack			3		uS
Quiescent Output Voltage	Vo	B=0G	2.25	2.5	2.75	V
Sensitivity	△Vout	TA=25℃	1.6	1.8	2.0	mV/G
Min Output Voltage		B=-1500G		0.86		V
Max Output Voltage		B=1500G		4.21		V

Figure A.3: SS49E Electrical Characteristics (TA = 25°C, VCC = 5V) [23]

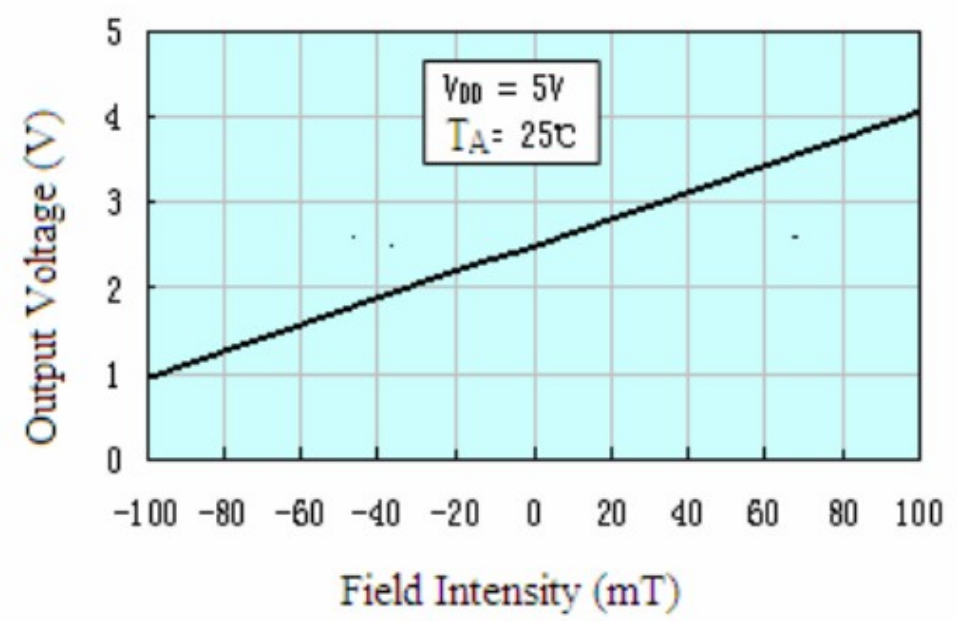

Figure A.4: SS49E Performance Characteristics [23]

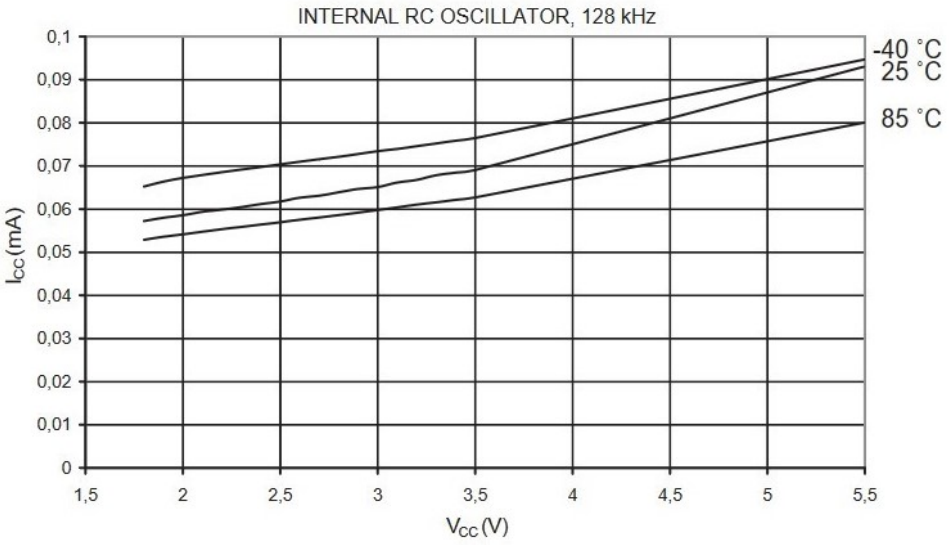

Figure A.5: ATtiny85 Idle Supply Current vs. Vcc [24].

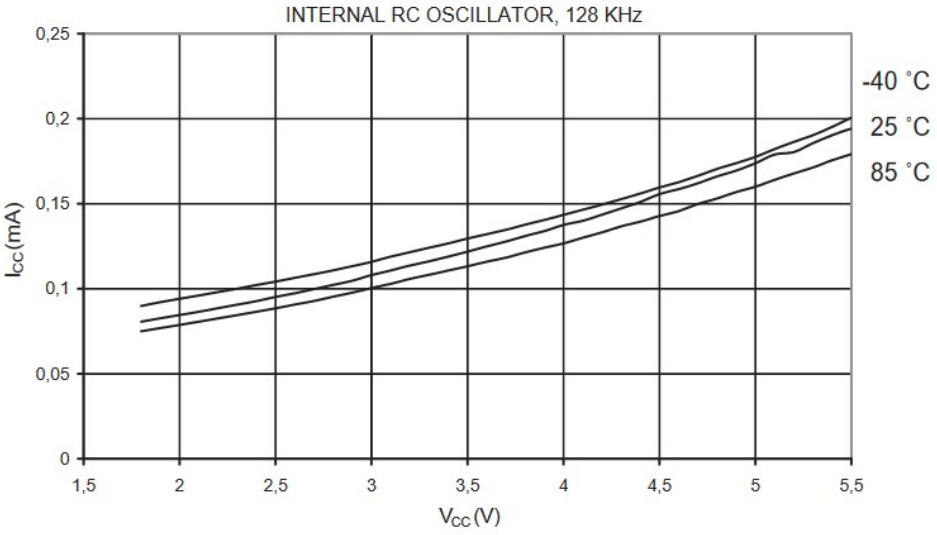

Figure A.6: ATtiny85 Active Supply Current vs. Vcc [24].

Symbol	Description	Conditions	Min	Typ	Max	Unit
IDDSL	Supply current in Sleep mode		-	0.2	1	uA
IDDIDLE	Supply current in Idle mode	RC oscillator enabled	-	1.5	-	uA
IDDST	Supply current in Standby mode	Crystal oscillator enabled	-	1.6	1.8	mA
IDDFS	Supply current in Synthesizer mode	FSRx	-	5.8	-	mA
IDDR	Supply current in Receive mode	*LnaBoost* Off, higher bands *LnaBoost* On, higher bands Lower bands	- - -	10.8 11.5 12.1	- - -	mA
IDDT	Supply current in Transmit mode with impedance matching	RFOP = +20 dBm, on PA_BOOST RFOP = +17 dBm, on PA_BOOST RFOP = +13 dBm, on RFO_LF/HF pin RFOP = + 7 dBm, on RFO_LF/HF pin	- - - -	120 87 29 20	- - - -	mA mA mA mA

Figure A.7: Electrical Specifications of the transceiver LoRa under the following conditions: Supply voltage VDD=3.3 V, T = 25°C, FXOSC = 32 MHz, FRF = 868 MHz, Pout=+13dBm [30].

Item	Specification
3.1 Nominal Capacity	2600mAh (0.2C, 2.75V discharge)
3.2 Minimum Capacity	2550mAh(0.2C, 2.75V discharge)
3.3 Charging Voltage	4.2 ±0.05 V
3.4 Nominal Voltage	3.7V
3.5 Charging Method	CC-CV (constant voltage with limited current)
3.6 Charging Current	Standard charge: 1300mA Rapid charge : 2600mA
3.7 Charging Time	Standard charge : 3hours Rapid charge : 2.5hours
3.8 Max. Charge Current	2600mA(ambient temperature 25℃)
3.9 Max. Discharge Current	5200mA(ambient temperature 25℃)
3.10 Discharge Cut-off Voltage	2.75V
3.11 Cell Weight	47.0g max
3.12 Cell Dimension	Height : 65.00mm max Diameter : 18.40mm max
3.13 Operating Temperature	Charge : 0 to 45℃ Discharge: -20 to 60℃
3.14 Storage Temperature	1 year : -20~25℃(1*) 3 months : -20~45℃(1*) 1 month : -20~60℃(1*)

Figure A.8: Battery Nominal Specifications [31].

Appendix B

In this appendix are provided the codes used for each instance and microcontroller.

B.1 Arduino Code

```
//Pin used to measure the sampling frequency. The frequency on this pin is
equal to half the sampling frequency
#define Fs 9
#define m 0.4053
#define dimensao 84
#define sensor 0 // A/D input where sensor signal conditioning is connected
bool flag = true;

// Initial state of the inv_notch filter
float u[3]={0.0,0.0,0.0};
float y[3]={0.0,0.0,0.0};

float quadrad_corrente_instantanea[dimensao];
float soma_quadrado_corrente_instantanea = 0;
float corrente_eficaz = 0;
float corrente_eficaz2 = 0;

int contador = 0;

void setup()
```

```
{
  Serial.begin(2000000);
  pinMode(Fs, OUTPUT);
  for (int i=0;i<dimensao;i++) quadrado_corrente_instantanea[i] = 0;
}

void loop()
{
  u[0] = (float)analogRead(sensor); // current sample

  //Filters data (removes DC and allows only 50Hz +/- 1Hz)
  y[0]= 1.89*y[1]-0.988*y[2]+0.00614*u[0]-0.00614*u[2];

  u[2]=u[1]; // Status update
  u[1]=u[0];
  y[2]=y[1];
  y[1]=y[0];

  // Calculates Effective Value
  // Fill vector with measurements
  quadrado_corrente_instantanea[contador]=y[0]*y[0];
  soma_quadrado_corrente_instantanea=0;
  for(int i=0;i<dimensao;i++) soma_quadrado_corrente_instantanea+=
  quadrado_corrente_instantanea[i];
  corrente_eficaz=(0.999*corrente_eficaz+0.001*
  sqrt(soma_quadrado_corrente_instantanea/dimensao));
  corrente_eficaz2=corrente_eficaz*m;

  contador++;
  contador=contador%dimensao;
  if (contador==0) Serial.println(corrente_eficaz2);
  //-------------------------------------------------------------------
  // To gauge the true sampling period
  if(flag)
  {
```

```
    digitalWrite(Fs,true);
    flag=false;
  }
  else
  {
    digitalWrite(Fs,false);
    flag=true;
  }
  //---------------------------------------------------------------------
}
```

B.2 ESP32 Code

```
//Pin used to measure the sampling frequency. The frequency on this pin is
equal to half the sampling frequency
#define Fs 26
#define dimensao 100 //Used to determine the RMS value of the signal
#define sensor 34 //A/D input where sensor signal conditioning is connected
#define m 0.0682

bool flag = true;

// Initial state of the inv_notch filter
float u[3]={0.0,0.0,0.0};
float y[3]={0.0,0.0,0.0};

float quadrado_corrente_instantanea[dimensao];
float soma_quadrado_corrente_instantanea = 0;
float corrente_eficaz = 0;
float corrente_eficaz2 = 0;

int contador = 0;
```

```
void setup()
{
  Serial.begin(1000000);
  pinMode(Fs, OUTPUT);
  for (int i=0;i<dimensao;i++) quadrado_corrente_instantanea[i] = 0;

}

void loop()
{
  u[0] = (float)analogRead(sensor); //Current sample
  //Filters data (removes DC and allows only 50Hz +/- 1Hz)
  y[0]= 1.89*y[1]-0.988*y[2]+0.00614*u[0]-0.00614*u[2];

  u[2]=u[1]; // Status update
  u[1]=u[0];
  y[2]=y[1];
  y[1]=y[0];

  // Calculates Effective Value
  // Fill vector with measurements
  quadrado_corrente_instantanea[contador]=y[0]*y[0];
  soma_quadrado_corrente_instantanea=0;

  for(int i=0;i<dimensao;i++)
    soma_quadrado_corrente_instantanea+=quadrado_corrente_instantanea[i];

  corrente_eficaz=0.999*corrente_eficaz+0.001*
  sqrt(soma_quadrado_corrente_instantanea/dimensao);
  corrente_eficaz2=m*corrente_eficaz;
  contador++;
  contador=contador%dimensao;

  Serial.println(corrente_eficaz2);
```

```
  //-------------------------------------------------------------------
  // To gauge the true sampling period
  if(flag)
  {
    digitalWrite(Fs,true);
    flag=false;
  }
  else
  {
    digitalWrite(Fs,false);
    flag=true;
  }
  delayMicroseconds(930);
  //-------------------------------------------------------------------
}
```

B.3 LoRa Sender with ATtiny85

```
#include <LoRa.h> // LoRa arduino library adapted for Attiny85

int counter = 0;

void setup()
{
  // Start loRa
  if (!LoRa.begin(868E6)) {
    while (1);
  }
}

void loop()
{
  // send LoRa packet every 1s
```

```
  LoRa.beginPacket();
  LoRa.print("- hello from tiny85 - ");
  LoRa.print("Packect # ");
  LoRa.print(counter);
  LoRa.endPacket();
  delay(1000);
  counter++;
}
```

B.4 Exponential Weighting Code

```
i_filtrado(k)=0.0581673384199269394*i_sensor(k)-0.0581673384199269394*
i_sensor(k-2)+ 1.52391725815133561*i_filtrado(k-1)-0.883665323160146121*
i_filtrado(k-2);
w(k)=lambda*w(k-1)+1;
// Calculates the RMS value based on the last h samples:
Irms(k) = (1-1/w(k))*Irms(k-1)^2 + (1/w(k))*i_filtrado(k)^2;
Irms(k)=sqrt(Irms(k));
```